

**Load effects in reinforced concrete beam bridges affected by alkali–silica reaction—Constitutive modelling including expansion, cracking, creep and crushing**

Kongshaug, Simen Sørgaard; Larssen, Rolf Magne ; Hendriks, Max A.N.; Kanstad, Terje; Markeset, Gro

**DOI**

[10.1016/j.engstruct.2021.112945](https://doi.org/10.1016/j.engstruct.2021.112945)

**Publication date**

2021

**Document Version**

Final published version

**Published in**

Engineering Structures

**Citation (APA)**

Kongshaug, S. S., Larssen, R. M., Hendriks, M. A. N., Kanstad, T., & Markeset, G. (2021). Load effects in reinforced concrete beam bridges affected by alkali–silica reaction—Constitutive modelling including expansion, cracking, creep and crushing. *Engineering Structures*, 245, 1-17. Article 112945. <https://doi.org/10.1016/j.engstruct.2021.112945>

**Important note**

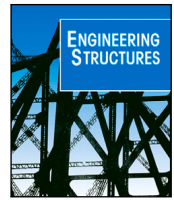
To cite this publication, please use the final published version (if applicable). Please check the document version above.

**Copyright**

Other than for strictly personal use, it is not permitted to download, forward or distribute the text or part of it, without the consent of the author(s) and/or copyright holder(s), unless the work is under an open content license such as Creative Commons.

**Takedown policy**

Please contact us and provide details if you believe this document breaches copyrights. We will remove access to the work immediately and investigate your claim.



# Load effects in reinforced concrete beam bridges affected by alkali–silica reaction—Constitutive modelling including expansion, cracking, creep and crushing

Simen Sørgaard Kongshaug<sup>a,c,\*</sup>, Rolf Magne Larssen<sup>b</sup>, Max A.N. Hendriks<sup>c,d</sup>, Terje Kanstad<sup>c</sup>, Gro Markeset<sup>a</sup>

<sup>a</sup> Oslo Metropolitan University, Pilestredet 35, 0130 Oslo, Norway

<sup>b</sup> Dr. Ing. A. Aas-Jakobsen AS, Lilleakerveien 4 A, 0283 Oslo, Norway

<sup>c</sup> Norwegian University of Sciences and Technology, Richard Birkelandsvei 1A, 7034 Trondheim, Norway

<sup>d</sup> Delft University of Technology, Stevinweg 1, 2628 CN Delft, The Netherlands

## ARTICLE INFO

### Keywords:

Reinforced concrete  
Alkali–silica reaction  
Imposed deformation  
Load effects  
Beam bridges  
Finite element analysis

## ABSTRACT

Material modelling, from the micro to the macro level, of concrete affected by alkali–silica reaction (ASR) has been devoted a lot of research. However, the application of the material models in structural analyses of reinforced concrete (RC) structures, showing the structural implications/consequences of ASR, has got little attention in the literature. This paper aims to show the relevance of the constitutive model on the calculated load effects—induced by ASR—in statically indeterminate beam structures. For the purpose of the study, a three-span RC beam, inspired by a real bridge in Norway, is analysed. The RC beam is modelled using Euler–Bernoulli beam theory, and numerical solutions are obtained with the finite element method. The effects of ASR on the concrete are accounted for in an expansion based (macro) constitutive model, which also accounts for cracking, creep and compressive non-linearity. In this way, ASR gives an imposed deformation similar to thermal dilation and shrinkage, for which structural effects have been widely studied. As imposed strain gradients tend to cause higher load effects than uniform strains, the effect of ASR gradients, owing to e.g. a moisture gradient, is addressed.

It is shown that linear structural analyses (using a linear material model), give conservative results (the greatest load effects) when an ASR strain gradient is imposed. Among the non-linear material effects investigated, it is shown that stress dependent ASR expansion and concrete cracking are important to consider. The stress dependency of the ASR expansion is shown to have a smoothing effect on the imposed ASR strain field, and as a result, reduces the load effects induced by ASR, while cracking results in crack/plastic hinges releasing the stresses in the system.

## 1. Introduction

This paper aims to illustrate the relevance of proper constitutive modelling of the effects of alkali–silica reaction (ASR) in combination with models for creep, cracking and reinforcement yielding, for the calculation of load effects in statically indeterminate beam structures. As an example, the structural analysis of a beam bridge with a reinforced concrete deck slab and with continuous multiple spans is selected.

ASR in concrete is an important deteriorating mechanism found in existing concrete structures all over the world. The effect of ASR is expansion and degradation of the material, most noticeable in terms of reduced modulus of elasticity and tensile strength, see e.g. the

experimental works [1–4] (Ref. [4] includes a collection of previous experimental results). On the structural level, the most noticeable signs of ASR are surface cracks and displacements leading to e.g. closing of expansion joints and skewed columns. In Norway, ASR in concrete structures was first identified and documented in the late 1970s (mainly in dams and swimming pools). However, it was not until early 1990s that ASR was accepted as a common deterioration process [5]. In 1996, regulations to prevent ASR in new structures were published. A relatively large number of concrete structures built before the mid-1990s, may therefore be constructed with an alkali–silica reactive concrete. Accordingly, ASR may be a potential problem

\* Corresponding author at: Oslo Metropolitan University, Pilestredet 35, 0130 Oslo, Norway.

E-mail address: [simkon@oslomet.no](mailto:simkon@oslomet.no) (S.S. Kongshaug).

URL: <https://oslomet.no> (S.S. Kongshaug).

<https://doi.org/10.1016/j.engstruct.2021.112945>

Received 12 February 2021; Received in revised form 20 July 2021; Accepted 27 July 2021

Available online 13 August 2021

0141-0296/© 2021 The Authors. Published by Elsevier Ltd. This is an open access article under the CC BY license (<http://creativecommons.org/licenses/by/4.0/>).

for many concrete structures in the coming decades, and the need for structural assessment follows.

An important structural assessment tool is the structural analysis, which is based on the theory of structural mechanics (solid continuum mechanics applied on structures). From a structural mechanical point of view, the effect of ASR can be considered and modelled as an imposed deformation [6–11] (reviews on modelling of ASR-affected concrete, on different levels and with different aims, are given in [12] and [13]). From other imposed deformations, like thermal expansion and shrinkage, we know that they may cause stresses (load effects), which is why imposed deformations are termed deformation loads. In contrast to thermal expansion, ASR will only cause expansion of the concrete (not the steel). Reinforcement bars will therefore have a restraining effect on the expanding concrete; this is similar to the effect of concrete shrinkage—but in the opposite direction and considerably larger. From expressions for the evolution of shrinkage strain and the variation in thermal strain ( $\pm 20$  °C), e.g. in Eurocode 2 [14], one finds that they are of one order smaller than the ASR expansion observed in experimental investigations (e.g. Ref. [1–4]), unless, the concrete is under sufficient compressive stress. Experimental investigations show that the ASR expansion is reduced with compressive stress [15–20]. The compressive stress that is required to stop the ASR expansion ranges between 3 to 10 MPa [21]. In addition to the local incompatibility of strain between concrete and reinforcement, differential ASR expansions/strains at structural level might occur, e.g. due to a moisture gradient as experimentally investigated by Multon et al. [22], where it was shown that a vertical moisture gradient gave rise to a vertical variation in the ASR-induced expansion. Besides, the rate of ASR (thus rate of expansion) is dependent on temperature, see e.g. Ref. [2]; so temperature variations may cause variations/gradients in the ASR-induced expansion. From heat and moisture transport characteristics in concrete, it can be argued that temperature variations are important for massive concrete structures as dams, while moisture variations are more important for slender structures as bridges [23,24]. In this way, temperature and moisture may play an important role in the spatial variation of ASR expansion even though thermal expansion and shrinkage are considered negligible. Considering the magnitude, the incompatibility between concrete and reinforcement, and the possibility of environmentally induced variations, it follows that ASR may cause significant additional stresses (load effects).

Structural assessment is often performed in a two-step procedure: (1) stresses (load effects) from different load combinations are first calculated (often with displacement based finite element method), and (2) load effects in cross sections are compared with capacities found in structural codes. In the first step, load effects are usually calculated based on assumptions leading to linear behaviour (linear equations), i.e. linear elasticity and small displacements. With these assumptions, load effects due to external loads (e.g. traffic loads) do not depend on the assumed modulus of elasticity, as long as the relative stiffness between all structural members remains invariant. In contrast, load effects due to imposed deformations (e.g. thermal dilation and ASR expansion) are highly dependent on the stiffness of the system, where in general, greater stiffness leads to larger load effects. Therefore, when imposed deformations are analysed, it is important that the structural model can represent the true rigidity. For instance, creep and cracking will highly affect the structural stiffness, and if these phenomena are present, they should be accounted for in the concrete material model. In addition, the influence of reinforcement on the structural stiffness must be accounted for.

Already in 1990, Courtier [6] proposed an engineering approach, for assessing the load effects in ASR-affected beams and columns. From the knowledge of expansion of concrete under varying compressive stress, and from elastic considerations, an expression for restrained expansion under varying reinforcement ratios was obtained, which was used in cross-sectional analyses of beams and columns to calculate the ASR-induced stress. It was further proposed how the method could be

extended to finite element analysis using the thermal strain feature. Since then (the last three decades), the research focus has shifted towards the constitutive modelling of ASR-affected concrete, and little attention is given to demonstrations showing the structural implications. Most of the demonstrations of the constitutive models are on either dams [9,11,25,26] or simply supported laboratory beams [8,10,24,27,28]. More recently a structural analysis of a Y-shaped pier of a highway bridge was conducted in [29]. No publications are found on ASR-induced load effects in multi span continuous RC beams (statically indeterminate beams).

This study is inspired by a real case, the Elgeseter Bridge in Norway, an ordinary RC beam bridge affected by ASR (a review of construction, research and repair up to 2003 is given in Ref. [5]). In 2012, large vertical cracks (6 mm) were observed in the inner beams, and spatial variations in ASR expansion were given as a possible explanation on the basis of signs of spatial moisture variations (visual inspection) and examination of plane polished sections [30]. Variations in moisture content in columns, one beam and the bridge deck are documented [5, 31]. Since the observation of the large vertical cracks, the structural effects of ASR expansion of the bridge superstructure have been the primary concern. To confirm the causality of the large cracks and to investigate the additional load effects of ASR, structural finite element analysis with focus on spatial variations of ASR expansion was conducted [32]. In a research and development programme, the Norwegian Public Roads Administration (NPRA), developed a guidance proposal for structural analysis of ordinary RC bridge superstructures [33], in which the Elgeseter Bridge is used as an example. Both of the previous attempts [32,33] can be considered as engineering approaches for assessing the load effects; the effect of ASR is modelled as an imposed concrete strain that is independent of stress, and use a stiffness that represents either uncracked or cracked concrete. These assumptions lead to a linear structural problem, which can be solved in most of the existing structural finite element programmes by the use of the thermal expansion feature. The simplicity and availability makes the method attractive, however, the consequences of such a simplified assumptions need further investigation. Besides, there is a discrepancy between these engineering approaches, and the more sophisticated material models for ASR-affected concrete proposed in the literature (see e.g. references mentioned above), where neglect of the stress dependence of the ASR expansion is considered as the most important one.

The objective of this paper is to increase the understanding of the effect of ASR expansion on the calculated load effects for ordinary RC continuous beams (statically indeterminate), which is important for assessing load effects in beam bridges. In particular, we want to explain the effect of ASR gradients (owing to e.g. a moisture gradient). Furthermore, we want to identify the aspects of the concrete constitutive model that have the most impact on the resulting load effects. As Courtier [6], we will view the matter from the practising engineer, and therefore, we will compare simplified assumptions (engineering approaches) with more sophisticated ones, to verify the consequence of simplifications. Where this paper focuses on the load effects, the consequence of ASR for the structural capacity is not investigated.

A numerical case study is performed on a generic three-span beam, inspired by the Elgeseter Bridge, to study the load effects due to ASR. The beams are modelled using Euler–Bernoulli beam theory with small displacements (geometric linearity), and non-linear material behaviour. The considered concrete material models differ in their complexity from the most simple one with linear elastic behaviour and stress independent ASR expansion, to including creep, cracking and stress dependent ASR expansion.

The findings in this paper emphasize the importance of proper ASR expansion modelling for predicting load effects. In addition, the study can support in developing guidelines for simplified structural assessment, which contribute to bridge the gap between engineering- and academic practice.

Section 2 describes the modelling of ordinary RC beams affected by ASR, with focus on the constitutive modelling of ASR-affected concrete. Sections 3–5 present the description, results, and discussion of the numerical case study.

## 2. Modelling of ordinary reinforced beams suffering from ASR

The kinematic assumptions are described in Section 2.1, while the material models for the concrete and the reinforcement are described in Sections 2.2 and 2.3, respectively.

The solutions to the structural problems investigated in this study are obtained with the displacement based finite element method (FEM), using 3-node (7 degrees of freedom) Euler–Bernoulli beam finite elements. Further details related to modelling (both physical, and numerical modelling in terms of FEM) of the case study are described in Section 3.

### 2.1. Kinematics

The following kinematic assumptions for the RC beams are made:

- deformation in accordance with Euler–Bernoulli beam theory, i.e. Navier’s hypothesis: cross sections before deformation remain planar and perpendicular to the deformed beam axis during deformation (also experimentally confirmed for ASR-affected RC beams [10]);
- small displacements;
- only displacements in the  $xz$ -plane (see Fig. 1);
- perfectly embedded reinforcement in the concrete, i.e. no slip. The strain in the reinforcement is uniform over the cross section, which means that the reinforcement’s resistance to bending is neglected.

The first three assumptions give the displacement field

$$\begin{bmatrix} u \\ w \end{bmatrix} = \begin{bmatrix} u_0(x) - z \frac{\partial w}{\partial x} \\ w(x) \end{bmatrix}, \quad (1)$$

where  $u_0$  is the displacement in the  $x$ -direction of particles initially positioned on the beam axis ( $x$ -axis is the beam/reference axis), and  $w$  is the displacement in the  $z$ -direction. This displacement field leads to only one non-zero strain component, which is the normal strain in the  $x$ -direction

$$\epsilon(x, z) = \frac{\partial u(x, z)}{\partial x} = \frac{\partial u_0(x)}{\partial x} - z \frac{\partial^2 w(x)}{\partial x^2}. \quad (2)$$

Eq. (2) shows that the (total) strain  $\epsilon$  is linear in  $z$ .

To include different concrete material effects, the total strain of the concrete is decomposed as

$$\epsilon = \epsilon^{\text{asr}} + \epsilon^\sigma + \epsilon^{\text{cr}} + \epsilon^{\text{creep}}, \quad (3)$$

where:

- $\epsilon^{\text{asr}}$  is the imposed ASR strain. It is a function of the free ASR strain  $\epsilon^{\text{asr,free}}$  (field variable), and stress, see Section 2.2.1 for the description of the constitutive model.
- $\epsilon^\sigma$  is the elastic strain, and represents the short term mechanical deformation. It is immediately reversible when the material is unloaded, thus elastic. Due to compressive softening, the loading path is non-linear, while the unloading is linear and follows the secant (hence energy dissipation). The constitutive model is described in Section 2.2.2
- $\epsilon^{\text{cr}}$  is the smeared crack strain, with the physical interpretation as a weaker/softer material that develops between the sound material. When a crack closes, the crack strain vanishes and the stiffness is recovered. The constitutive model is described in Section 2.2.3.
- $\epsilon^{\text{creep}}$  is the creep strain. This is the time dependent deformation due to stress; for a constant stress it increases with time. The constitutive model is described in Section 2.2.5.

Similar decomposition of concrete strain, including creep strain, can be found elsewhere [34,35].

The total strain of the reinforcement is also decomposed. To account for yielding, it is decomposed into an elastic and a plastic strain component:

$$\epsilon = \epsilon^{\text{el}} + \epsilon^{\text{pl}}. \quad (4)$$

The constitutive model of the reinforcement is described in Section 2.3.

### 2.2. Constitutive model for ASR-affected concrete

#### 2.2.1. ASR expansion model

The effect of ASR is modelled on the concrete material level, where we use an expansion based model similar to a model proposed by Wen [8]. The expansion model is based on the following assumptions:

- The free ASR expansion  $\epsilon^{\text{asr,free}}$ —different from the imposed one—is a predefined field variable, i.e. a known function of space and time; it is a measure that represents the ASR strain that would occur without stress.
- The imposed expansion  $\epsilon^{\text{asr}}$  depends on the stress, given by the instantaneous stress–expansion relationship

$$\dot{\epsilon}^{\text{asr}} = W(\sigma) \dot{\epsilon}^{\text{asr,free}}. \quad (5)$$

In Eq. (5), the over-dot denotes the time derivative, and  $W$  is a function of stress that takes a value in  $[0, 1]$ ;  $W$  must be constructed such that compressive stress reduces the expansion, while tensile stress does not influence the expansion ( $W = 1$  for  $\sigma > 0$ ). It should be noted that  $W(\sigma)$  remains unchanged during the whole expansion process, i.e. it is not a function of time.

- The imposed expansion  $\epsilon^{\text{asr}}$  in any particular direction depends only on the stress in the same direction, i.e. the stress in the longitudinal direction of the beam has no influence on the expansions perpendicular to the beam, and vice versa. The use of beam theory is, therefore, consistent with this assumption.

The validity of the last assumption depends (amongst other) on the concrete mix as different anisotropic expansion behaviours have been reported in the literature. Four expansion behaviours can be identified—if at least one direction is free of stress: (1) total transfer of expansion to the stress-free directions, i.e. volumetric expansion is preserved [2,16,36,37], (2) partial transfer of expansion [17–19], (3) no or negligible transfer to the stress-free directions [15,38], and (4) the expansion in the stress-free directions is reduced [39,40]. The expansion model, used in this study, is compliant with expansion behaviour (3).

Different instantaneous stress–expansion relationships, i.e. various functions  $W$  in (5), are investigated:

- Stress independent ASR expansion.* This means that  $W = 1$  for all  $\sigma$ , and consequently, the imposed expansion field equals the free ASR expansion field:  $\epsilon^{\text{asr}} = \epsilon^{\text{asr,free}}$ . This assumption makes it possible to use the thermal dilation feature that exists in most of the FEM softwares to model the ASR expansion. The simplicity and availability makes the method attractive for the consulting engineer. However, the consequences of this simplified expansion behaviour needs investigation, and is, therefore, compared to more experimentally sound expansion behaviours (given in (b)).
- Stress dependent ASR expansion of varying degree.* Two functions  $W(\sigma)$  are investigated: the logarithmic function proposed by Charlwood et al. [7], Eq. (6), and a linear function, Eq. (7), both illustrated in Fig. 2.

$$W_{\text{ch}}(\sigma) = \begin{cases} 1 & \text{if } \sigma \geq -\sigma_L \\ 1 - \frac{\log(\sigma/-\sigma_L)}{\log(\sigma_u/-\sigma_L)} & \text{if } -\sigma_u \leq \sigma < -\sigma_L \\ 0 & \text{if } \sigma < -\sigma_u \end{cases} \quad (6)$$

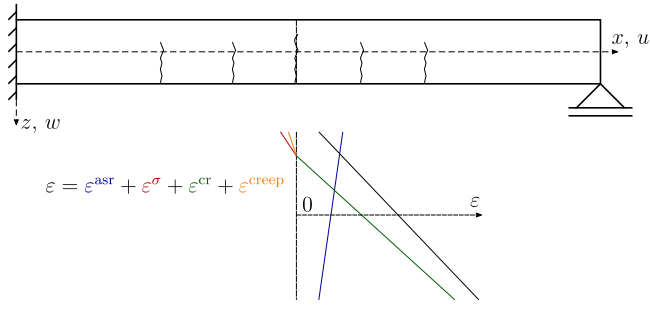


Fig. 1. The beam deforms in accordance with Navier's hypothesis which makes the total strain  $\epsilon$  linear in  $z$  (black line). The other strain components, however, might be non-linear in  $z$ . The figure shows one possible decomposition of  $\epsilon$  for a cross section.

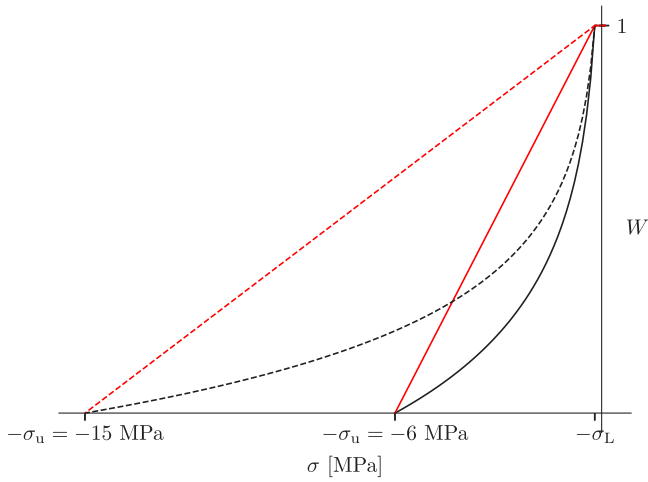


Fig. 2. The weight function originally proposed by Charlwood [7] in black, the linear function in red.

$$W_{\text{lin}}(\sigma) = \begin{cases} 1 & \text{if } \sigma \geq -\sigma_L \\ \frac{\sigma + \sigma_u}{\sigma_u - \sigma_L} & \text{if } -\sigma_u \leq \sigma < -\sigma_L \\ 0 & \text{if } \sigma < -\sigma_u \end{cases} \quad (7)$$

The material constant  $\sigma_u$  is an upper compressive stress bound, i.e. the stress for which the ASR expansion rate stops, and the material constant  $\sigma_L$  is the lower compressive stress bound, i.e. the stress for which the ASR expansion rate equals the free ASR expansion rate. These material constants are uncertain and depend, among other things, on the concrete mix, and must be determined from restrained expansion experiments. The study of Berra et al. [17] showed that the restrained expansion under a compressive stress of 0.17 MPa was similar to the corresponding unrestrained expansion, irrespective of concrete mix. Therefore, we have chosen the lower compressive bound  $\sigma_L = 0.2$  MPa. In our study, we have investigated the influence of the upper compressive bound, where two values are chosen:  $\sigma_u = \{6, 15\}$  MPa, where 6 MPa is within in the range of experimental observations, see e.g. [15], and 15 MPa is somewhat larger than what experimentally observed to study the effect of the upper compressive bound.

### 2.2.2. Elastic compliance relation accounting for ASR and compressive damage

In this study, the elastic strain  $\epsilon^\sigma$  represents the instant deformation due to stress, and it is given by the following compliance relation:

$$\epsilon^\sigma = C^\sigma \sigma. \quad (8)$$

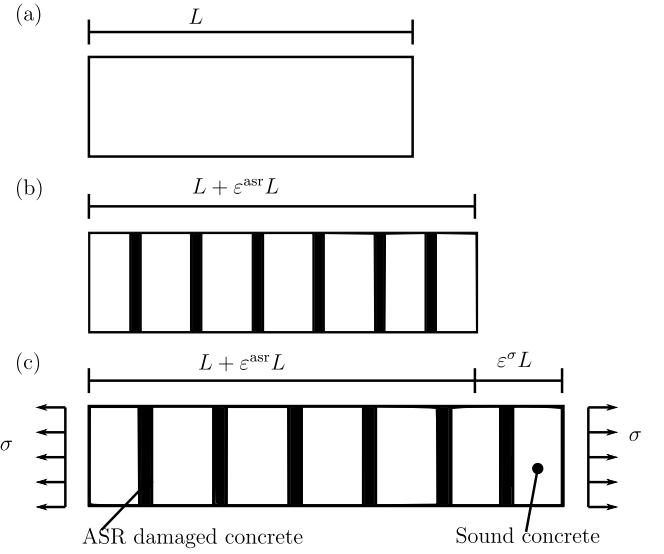


Fig. 3. Illustration of the series model for ASR-affected concrete: (a) concrete fibre of initial length  $L$ , (b) expands  $\epsilon^{\text{ASR}} L$  due to ASR, and (c) it strains  $\epsilon^\sigma L$  due to stress  $\sigma$ .

To account for the increase in compliance (or reduction in stiffness) due to ASR, a series model inspired by the work of [8] is used, where the ASR-affected concrete is considered as being composed of sound concrete and ASR damaged concrete in series, see Fig. 3. The sound concrete has an initial stiffness equal to the modulus of elasticity  $E_0$ , and the damaged concrete has a reduced modulus of elasticity  $E_{\text{asr}} = \beta_E^{\text{asr}} E_0$ , where  $\beta_E^{\text{asr}}$  is a coefficient. Furthermore, it is assumed that a concrete material fibre with initial length  $L$  (Fig. 3a) expands  $L_{\text{asr}} = \epsilon^{\text{asr}} L$  (Fig. 3b) due to ASR. Based on these assumptions, the change of length of the composite under stress (Fig. 3c) is composed of two parts, given by

$$\begin{aligned} \epsilon^\sigma L &= \epsilon^{\sigma, \text{sound}} L + \epsilon^{\sigma, \text{asr}} L_{\text{asr}} \\ &= C^{\sigma, \text{sound}} \sigma L + \frac{\sigma}{E_{\text{asr}}} L_{\text{asr}} \\ &= C^{\sigma, \text{sound}} \sigma L + \frac{\sigma}{\beta_E^{\text{asr}} E_0} \epsilon^{\text{asr}} L, \end{aligned} \quad (9)$$

where  $\epsilon^{\sigma, \text{sound}}$  is the elastic strain of the sound concrete,  $\epsilon^{\sigma, \text{asr}}$  is the elastic strain of the damaged concrete, and  $C^{\sigma, \text{sound}}$  is the elastic compliance of sound concrete. Division by  $L$ , leads to the following expression for the elastic strain

$$\begin{aligned} \epsilon^\sigma &= \left( C^{\sigma, \text{sound}} + \frac{\epsilon^{\text{asr}}}{\beta_E^{\text{asr}} E_0} \right) \sigma \\ &= \underbrace{\left( C^{\sigma, \text{sound}} + C^{\sigma, \text{asr}}(\epsilon^{\text{asr}}) \right)}_{C^\sigma} \sigma. \end{aligned} \quad (10)$$

By comparing Eq. (8) with (10), we can identify the expression for the elastic compliance  $C^\sigma$ . Notice that the second term  $C^{\sigma, \text{asr}}$  is linearly increasing with ASR expansion, but constant with respect to stress. This means that the concrete stiffness is gradually reduced with ASR expansion.

Initially, the elastic compliance of the sound concrete is  $C^{\sigma, \text{sound}} = 1/E_0$ . To account for compressive damage, we will later show how it increases with loading. For now, let us assume that it has its initial value. Then, if we solve Eq. (10) with respect to the stress, we obtain

$$\sigma = \underbrace{\left( 1 - \frac{\epsilon^{\text{asr}}}{\epsilon^{\text{asr}} + \beta_E^{\text{asr}}} \right)}_E E_0 \epsilon^\sigma. \quad (11)$$

In Eq. (11), the damaged modulus of elasticity  $E$  is defined. The relative modulus of elasticity  $E/E_0$  is, therefore, the expression in parentheses.

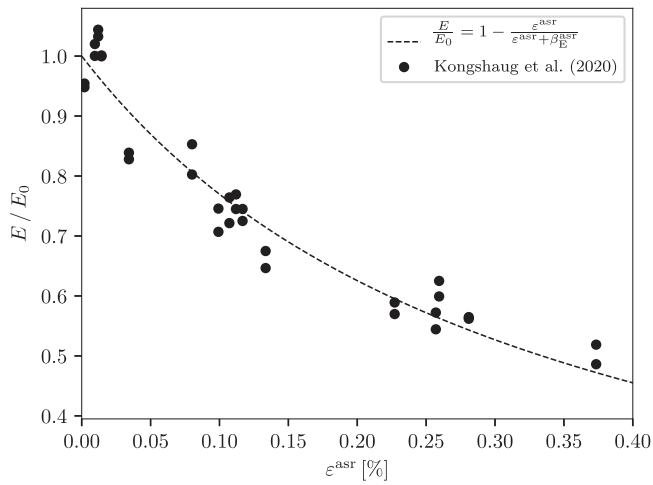


Fig. 4. Evolution of relative modulus of elasticity from [20].

The evolution of relative modulus of elasticity was experimentally investigated by Kongshaug et al. [20]. The coefficient  $\beta_E^{\text{ASR}} = 0.0033$  gave the best fit to the experimental data obtained from the stiffness damage test (SDT, [41]), these results are shown in Fig. 4. In the same study, the modulus of elasticity (defined as the secant stiffness at 40% of the compressive strength) obtained from the measurement of the complete stress–strain relationship—tested in another machine—gave  $\beta_E^{\text{ASR}} = 0.0038$  as the best fit.

It can be shown that the ASR damage model described above is equivalent to the model used in the work of [27,42,43] and [44], where the value of  $\beta_E^{\text{ASR}} = 0.003$  was used.

The stress–strain curves (to peak stress) obtained by Kongshaug et al. [20], for ASR expansion of varying degree, are shown in Fig. 5a. For now, assume that the elastic strain  $\epsilon^\sigma$  (in our model) corresponds to the measured strain  $\epsilon^\sigma$  in Fig. 5a. If we subtract the elastic strain of the ASR damaged material  $\epsilon^{\sigma,\text{ASR}} = C^{\sigma,\text{ASR}}\sigma$ , with  $\beta_E^{\text{ASR}} = 0.0038$  and  $E_0 = 24\,302$  MPa, we obtain the stress–strain curves in Fig. 5b. The strain along the horizontal axis now corresponds to the elastic strain of the sound material  $\epsilon^{\sigma,\text{sound}}$ . It is interesting that these curves are similar, with almost the same peak strain. Therefore, we conclude that the effect of ASR expansion as an increase in compliance ( $C^{\sigma,\text{ASR}}$ ) that is independent of the loading, is a reasonable approach.

In terms of the series model, the compressive damage applies to the sound/undamaged part, and therefore, it is independent of the ASR expansion. It is accounted for by making the elastic compliance of the sound part  $C^{\sigma,\text{sound}}$  (the first term in Eq. (10)) dependent on the loading. It is given by

$$C^{\sigma,\text{sound}} = \begin{cases} \frac{1}{E_0} & \text{for } \alpha^c = 0 \\ \frac{\alpha^c}{\sigma^c(\alpha^c)} & \text{for } \alpha^c > 0 \end{cases}, \quad (12)$$

where  $\frac{\alpha^c}{\sigma^c(\alpha^c)}$  is the secant compliance to the compressive stress–strain curve ( $\sigma^c(\alpha^c)$ ) for a non-reacted concrete, see Fig. 6. The state variable  $\alpha^c$  depends on the compressive strain and equals, in absolute sense, the minimum value of  $\epsilon^{\sigma,\text{sound}}$  during the history;  $\alpha^c = |\min(\epsilon^{\sigma,\text{sound}})|$ . The compressive curve/function  $\sigma^c$  proposed by Popovic [45] is used:

$$\sigma^c = \left( \frac{\alpha^c}{\epsilon_{c0}} \right) \frac{n}{n-1 + \left( \frac{\alpha^c}{\epsilon_{c0}} \right)^n} f_c; \quad (13)$$

$$n = \frac{1}{1 - \frac{f_c}{\epsilon_{c0}E_0}},$$

where  $f_c$  is the compressive strength, and  $\epsilon_{c0}$  is the peak compressive strain.

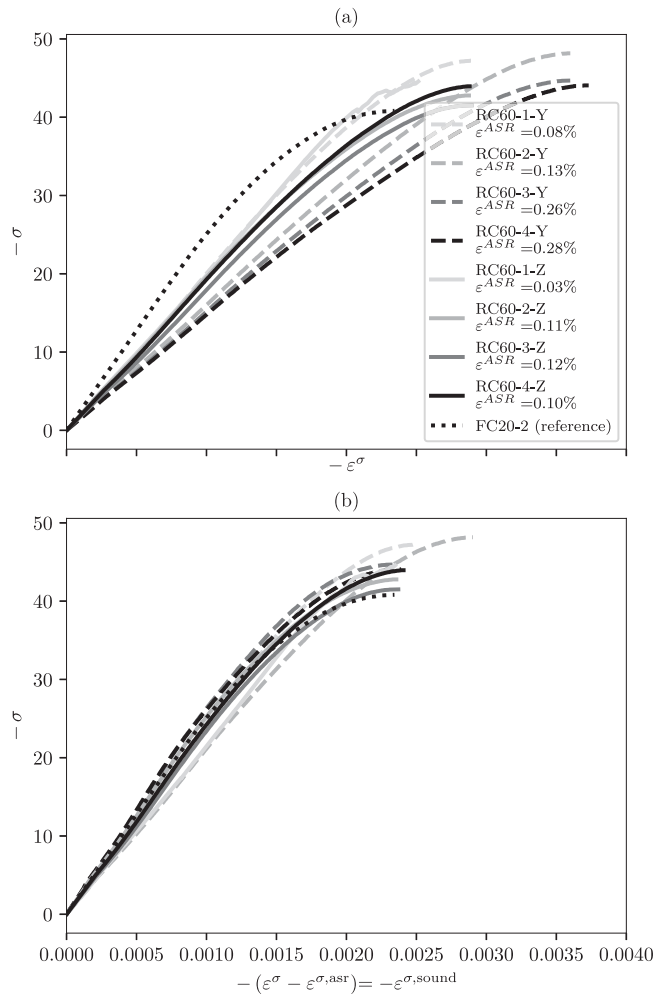


Fig. 5. (a) Compressive stress–strain curves from [20], and (b) the strain is modified by removing the elastic strain of the ASR damaged material  $\epsilon^{\sigma,\text{ASR}}$ .

The evolution of compressive damage, i.e.  $\dot{\alpha}^c \geq 0$ , is controlled by the compressive damage criterion, given by

$$F^c = -\sigma - \sigma^c(\alpha^c) \leq 0, \quad (14)$$

where the loading/unloading conditions are given by

$$\dot{\alpha}^c \geq 0, \quad F^c \dot{\alpha}^c = 0. \quad (15)$$

The material is loaded when  $\dot{\alpha}^c > 0$ , whereas  $\dot{\alpha}^c = 0$  when it the material is unloaded/reloaded. The strain–stress relation in compression is demonstrated in Fig. 6 for  $f_c = 28$  MPa,  $\epsilon_{c0} = 0.002$ , and  $E_0 = 23\,313$  MPa. One observes that the compressive stress is limited by  $\sigma^c$ , and the unloading/reloading is linear along the secant line.

### 2.2.3. Cracking model

The smeared crack strain  $\epsilon^{\text{cr}}$  is given by the following compliance relation

$$\epsilon^{\text{cr}} = C^{\text{cr}} \sigma, \quad (16)$$

where the compliance is given by

$$C^{\text{cr}}(\alpha^{\text{cr}}) = \begin{cases} \frac{\alpha^{\text{cr}}}{\sigma^{\text{cr}}(\alpha^{\text{cr}})} & \text{for } \sigma > 0. \\ 0 & \text{for } \sigma \leq 0 \end{cases}; \quad (17)$$

$$\alpha^{\text{cr}} = \max(\epsilon^{\text{cr}}).$$

From the above expression, one can see that crack closing is accounted for by a vanishing crack compliance  $C^{\text{cr}}$  when the stress is negative. The

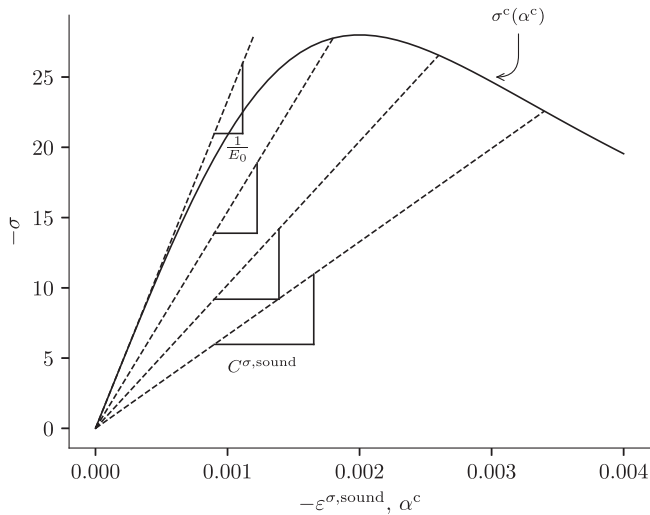


Fig. 6. Compressive stress–strain curve  $\sigma^c$  of Popovics [45], and the evolution of the compliance  $C^{\sigma,\text{sound}}$ .

current concrete tensile strength is given by  $\sigma^{\text{cr}}$ . In general, it could be a decaying function of the internal state variable  $\alpha^{\text{cr}}$  such that both concrete tension softening and tension stiffening are accounted for. However, in this paper we have for simplicity assumed brittle fracture with a small residual stress, given by

$$\sigma^{\text{cr}} = \begin{cases} f_{\text{ct}} & \text{if } \alpha^{\text{cr}} = 0 \\ 0.01f_{\text{ct}} & \text{if } \alpha^{\text{cr}} > 0 \end{cases}, \quad (18)$$

where  $f_{\text{ct}}$  is the tensile strength. The evolution of cracking, i.e.  $\dot{\alpha}^{\text{cr}} \geq 0$ , is controlled by the cracking criterion, given by

$$F^{\text{cr}} = \sigma - \sigma^{\text{cr}}(\alpha^{\text{cr}}) \leq 0, \quad (19)$$

where the loading/unloading conditions are given by

$$\dot{\alpha}^{\text{cr}} \geq 0, \quad F^{\text{cr}} \dot{\alpha}^{\text{cr}} = 0. \quad (20)$$

#### 2.2.4. Demonstration of the short-term stress–strain relationship

The concrete material model (presented so far) is demonstrated in Fig. 7, where the material is first stretched, leading to cracking (grey line), and then unloaded, which results in crack closing (red line). The material is further compressed with an recovered initial stiffness (black line). After a certain compressive straining and damage, the material is unloaded and reloaded (blue secant), and finally compressed until failure when  $\alpha_c = \epsilon_{\text{cu}}$  (marked with a star).

#### 2.2.5. Creep deformation

Time dependent deformation of concrete under sustained loading, known as creep, depends on the age at loading, which is attributed to the degree of hydration of the cement paste; we say that concrete is an ageing material. Pourbehi et al. [44] emphasize (in their conclusion) the importance of including creep strains in an assessment study of an ASR-affected structure, which we will do in this study. In a recent experimental investigation, Reinhardt et al. [46] studied creep deformation of concrete mixes with slowly alkali–silica reactive aggregates. They found that creep behaviour was related to the expansion rate of concrete, where greater expansion rate resulted in greater creep deformation. This was explained by the degree of disorder of the particles, such that the greatest disorder coincides with the highest expansion rate and consequently, the highest creep rate. This suggests that there is an ageing effect related to ASR—in addition to the ageing effect of hydration. In Ref. [46], the concrete was first damaged by ASR in stress-free conditions and then exposed to sustained load for creep measurement. In RC damaged structures, ASR develops in presence

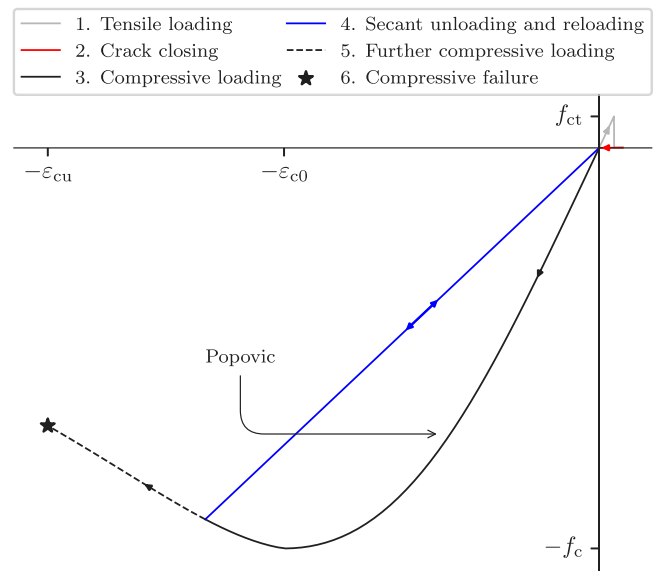


Fig. 7. Non-linear material model for short term loading (i.e. without creep and ASR deformation).

of restraint, and thus in presence of compressive stress. The effect of ASR on concrete creep should be different in these two situations. Due to the much lower expansion rate in-situ of reinforced concrete structures compared to accelerated experiments, we neglect the effect of expansion rate on creep.

In this study, concrete creep is modelled in two ways: (1) concrete is assumed as an ageing linear viscoelastic material, and (2) creep is assumed to give a constant increase in compliance, which corresponds to the effective modulus method. In the following, we also assume that the structure is stress free up to concrete age of 28 days, and therefore, we introduce the time variable  $t$ , which measures the time, in days [d], from 28 days after casting. In the first creep model, the creep strain at time  $t$  due to a stress history  $\sigma(\tau)$  is

$$\epsilon^{\text{creep}}(t) = \int_{\tau=0}^t C^{\text{creep}}(t, \tau) \sigma d\tau, \quad (21)$$

where  $C^{\text{creep}}(t, \tau)$  is the creep function, and  $\tau$  is the time at loading, also measured in days from 28 days after concrete casting. In the second model, the creep strain at time  $t$  is obtained by assuming a constant value of the creep function  $C^{\text{creep}}$ , which simplifies Eq. (21) to

$$\epsilon^{\text{creep}}(t) = C^{\text{creep}} \sigma(t). \quad (22)$$

In both methods, the Eurocode creep model [14] is assumed, i.e. the creep function given by

$$C^{\text{creep}}(t, \tau) = \frac{\phi(\hat{t}, \hat{\tau})}{E_0}, \quad (23)$$

Note that the creep coefficient  $\phi(\hat{t}, \hat{\tau})$  from Eurocode is given in terms of the time variables  $\hat{t}$  and  $\hat{\tau}$  given in days after casting, so  $\hat{t} = t + 28$  d and  $\hat{\tau} = \tau + 28$  d. In the second creep model, a choice of a constant value of the creep coefficient must be made, or rather, the choice of the time variables  $\hat{t}$  and  $\hat{\tau}$  used to calculate the creep coefficient. When the creep coefficient  $\phi$  is constant, the creep strain at time  $t$  is given by

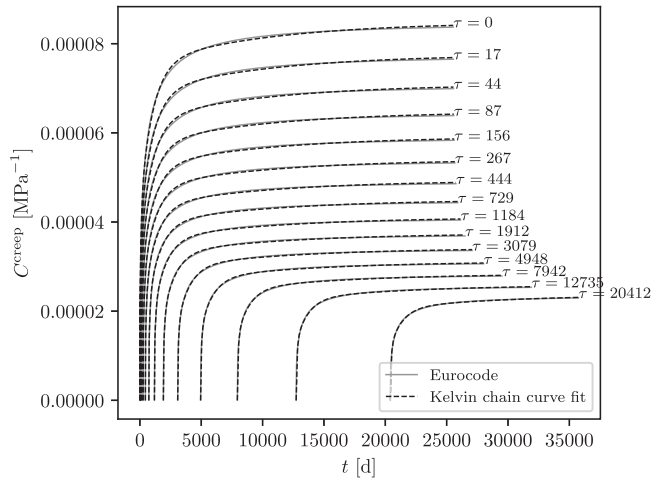
$$\epsilon^{\text{creep}}(t) = \frac{\phi}{E_0} \sigma(t). \quad (24)$$

To obtain a numerically effective solution procedure (for the first creep model), a five-unit Kelvin chain is fitted to the Eurocode creep function with the least squares method. The creep strain at time  $t$  modelled with the five-unit Kelvin chain is

$$\epsilon^{\text{creep}}(t) = \int_{\tau=0}^t \sum_k^5 \frac{1}{E_k^{\text{creep}}(\tau)} (1 - e^{-\frac{t-\tau}{\lambda_k}}) \sigma d\tau, \quad (25)$$

**Table 1**Input parameters to obtain the Eurocode creep function,  $C(t, \hat{t})$ .

Input parameters	Value
Mean value of concrete cylinder compressive strength, $f_{cm}$ [N/mm <sup>2</sup> ]	28
Tangent modulus of elasticity at an age of 28 days, $E_0$ [N/mm <sup>2</sup> ]	23313
Relative Humidity, RH [%]	80
Notional size, $h_0$ [mm]	700

**Fig. 8.** Eurocode creep functions [14] and the corresponding Kelvin chain curve fit for 15 times at loading.

where  $\lambda_k$  is the retardation time of unit  $k$  of the Kelvin chain. The objective of the curve fitting is, therefore, to approximate  $\frac{\phi(\hat{t}, \hat{t})}{E_0}$  with  $\sum_{k=1}^5 \frac{1}{E_k^{\text{creep}}(\tau)} (1 - e^{-\frac{\tau}{\lambda_k}})$ . In the approximation method, the retardation times are assumed constant, and equally spaced in the logarithmic scale, given by

$$(\lambda_1, \lambda_2, \lambda_3, \lambda_4, \lambda_5) = (1, 10, 100, 1000, 10000)\text{days}. \quad (26)$$

Then, the five compliances  $1/E_k^{\text{creep}}$  ( $k = 1, 2, 3, 4, 5$ ) are determined with the least squares method for different times at loading  $\tau_1, \tau_2, \dots, \tau_N$  equally spaced in the natural logarithm. For each considered time at loading  $\tau_i$ , the least square condition is imposed on point values  $t_1, t_2, \dots, t_j, \dots, t_M$ , where all  $t_j$  are selected in the range  $[\tau_i, t_{\text{end}}]$ , equally spaced in the natural logarithm, and  $t_{\text{end}}$  is the time at the end of the structural analysis. When the set of compliances for each time at loading is found, another curve fit is conducted, on this set, to obtain an approximation for the evolution of each compliance (i.e. the ageing property) where the following model function is assumed:

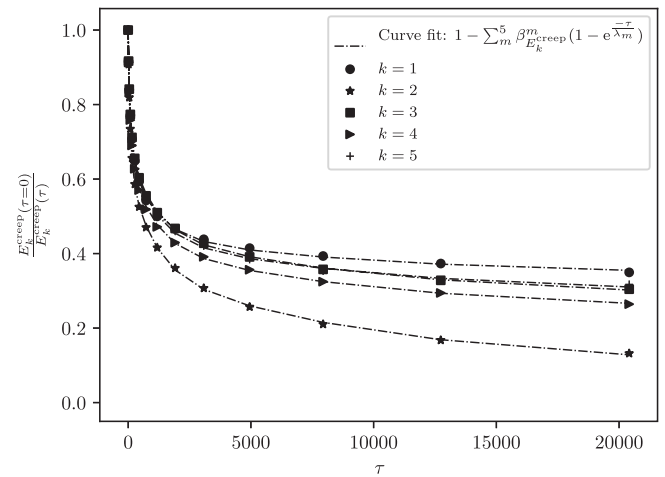
$$\frac{1}{E_k^{\text{creep}}(\tau)} = \left( 1 - \sum_{m=1}^5 \beta_m^{\text{creep}} (1 - e^{-\frac{\tau}{\lambda_m}}) \right) \frac{1}{E_k^{\text{creep}}(\tau=0)} \quad (27)$$

To demonstrate the curve fitting, we assume the input values in Table 1 to obtain a creep function  $C^{\text{creep}}(t, \tau) = \frac{\phi(\hat{t}, \hat{t})}{E_0}$  from Eurocode. The result of the curve fit is shown in Fig. 8, where one least square procedure is invoked for each of the 15 times at loading shown in the figure. Fig. 9 shows the result of the curve fit for the evolution of compliances for each Kelvin unit, shown in relative value to the compliance at  $\tau = 0$  (or  $\hat{t} = 28$ ).

### 2.3. Constitutive model for the reinforcement

The reinforcement is modelled using classical plasticity theory, in which the stress is given by Hook's law:

$$\sigma = E_s(\epsilon - \epsilon^{\text{pl}}), \quad (28)$$

**Fig. 9.** Curve fit for the evolution of each compliance relative value to the compliance at  $\tau = 0$  of the five Kelvin units.

where  $E_s$  is the modulus of elasticity of the steel, and  $\epsilon^{\text{pl}}$  is the plastic strain. The yield criterion is given by

$$F^{\text{pl}} = |\sigma| - \sigma^{\text{pl}}(\kappa) \leq 0, \quad (29)$$

where  $\sigma^{\text{pl}}$  is the yield strength which depends on the hardening variable  $\kappa$ . The yield strength is given by the hardening law:

$$\sigma^{\text{pl}} = f_{\text{sy}} + S \kappa, \quad (30)$$

where  $f_{\text{sy}}$  is the initial yield strength, and  $S$  is the hardening modulus. The flow rule is given by

$$\dot{\epsilon}^{\text{pl}} = \dot{\lambda} \text{sign}(\sigma); \quad \dot{\lambda} \text{ is the plastic multiplier.} \quad (31)$$

The strain hardening hypotheses is employed, i.e.  $\dot{\lambda} = \dot{\kappa}$ , and the loading/unloading conditions are

$$\dot{\lambda} \geq 0, \quad F^{\text{pl}} \dot{\lambda} = 0. \quad (32)$$

### 3. Numerical case study

Our study is inspired and motivated by a real case, Elgeseter Bridge in Norway, which is affected by ASR; the case is described in Section 3.1. Based on the knowledge of Elgeseter Bridge, and for the purpose of this study, we created a simplified and more generic version, and an associated beam model, described in Section 3.2. Further details about modelling and analysis of the generic case, and description of the investigated load cases, are given in Section 3.3.

#### 3.1. Description of the inspirational and motivational case: Elgeseter bridge

Elgeseter Bridge in Norway was built in 1951, and is an important infrastructure in the city centre of Trondheim. In 2008, it was listed by the Norwegian Heritage board. It is a 200m long ordinary RC beam bridge. The slab is carried by four longitudinal beams, which are supported by slender columns, see Fig. 10; everything is made of monolithically cast reinforced concrete. The reinforcement consists of plain (without ribs) ordinary steel. The reinforcement layout, shown in Fig. 11, is well designed for the known load conditions: self-weight and traffic load.

In the recent years, the structural effects of ASR expansion of the bridge superstructure have become the primary concern [32,33]. ASR has resulted in an elongation of the bridge, which has been quantified through measurements of the width of the only expansion joint in the north end of the bridge—designed to be 200 mm wide. In 2003, the width was reduced to near zero, which made repair of the expansion

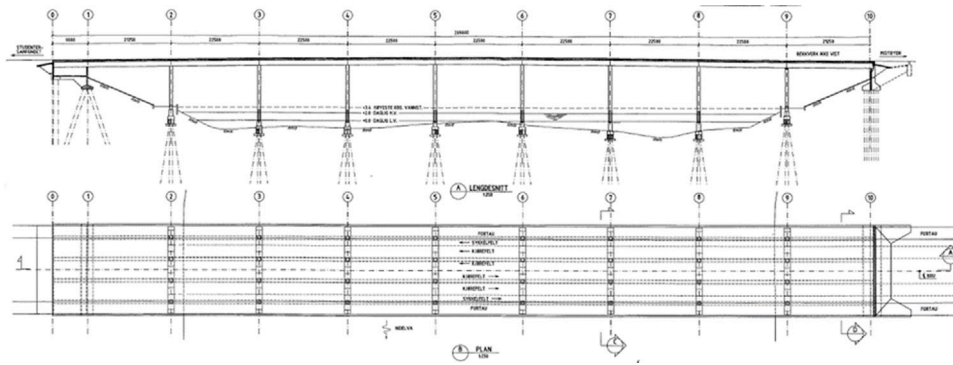


Fig. 10. Drawing of Elegeseter bridge [32].

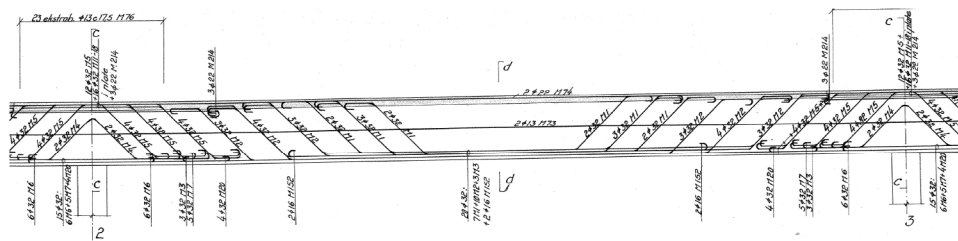


Fig. 11. Drawing of the reinforcement in the beams of Elegeseter bridge [32].



Fig. 12. Signs of water penetration of the bridge deck in outermost region of the bridge. Image courtesy of Dr. Ing. A. Aas-Jakobsen AS.

joint necessary. Based on the expansion joint measurements from 1962 to 2001, reported in [32], the current elongation of the bridge is estimated at 200 mm, which gives an average expansion of 0.1%. From an inspection of the bridge in 2012 [30], it was observed that water penetrated through the bridge deck, likely due to punctuation of the water sealing, in the outermost part of the bridge on both sides, and throughout the bridge length, see Fig. 12. It has been believed, that this has resulted in a spatial moisture variation over both the height and the width, and therefore, variations in ASR expansion [32]. A variation in water content in the width of the bridge deck is documented [31].

Large vertical cracks were observed on the bridge in 2012 [30], see Fig. 13, and were explained by the ongoing ASR deformations [32]. These cracks have occurred in cross sections with low amounts of reinforcement, where the bending moments due to self-weight are low.

### 3.2. The three-span beam and the associated structural model

A simplified version of the real case is constructed: a three-span beam with similar geometry to one of the beams in the last three spans of Elegeseter Bridge, see Fig. 14. The reinforcement layout is simplified to only one layer in the top, and one in the bottom of the cross section (see Fig. 14). The reinforcement layout for the whole length of the three-span beam is given in Table 2. Similar to the observation on Elegeseter, it is assumed that the average expansion of the three-span beam reaches 0.1% after 70 years, which results in an elongation of 66 mm. It is also assumed that a vertical moisture gradient, as observations on Elegeseter Bridge indicate, causes a linear variation in the free ASR expansion (which is used as a predefined field variable).

The three-span beam is modelled as described in Section 2. The span lengths, the boundary conditions, and the line load (representing the permanent loads), are shown in Fig. 15. The line load  $q$ , was derived by matching the results from a structural analysis of the complete bridge [32]. As the bridge geometry is repetitive for each span, except the end span, the three-span beam model is adequate to give a sufficient representation of the total bridge for ordinary loading; the structural analyses of the complete bridge shows that the results in span three from the right (with reference Fig. 10) are repetitive, while the results in the last two spans differ from the rest of the bridge due to support conditions and geometry.

### 3.3. Further details about modelling and analysis, and description of load cases

The three-span beam is meshed into finite elements of length 1 m, except some elements of 1.5 m to match the reinforcement layout. Thirteen integration points over the height of the beam is selected for the integration of the concrete stress, in addition to two integration points for the reinforcement, i.e. one for each reinforcement layer.

Each analysis is split into two steps, where permanent load is applied as a line load  $q = 86.67 \text{ N/mm}$  in the first step (over a very short time). In the second step, a predefined free ASR strain field is linearly increased over the bridge age until the axial displacement at the end of the beam reaches 66 mm, which corresponds to an average

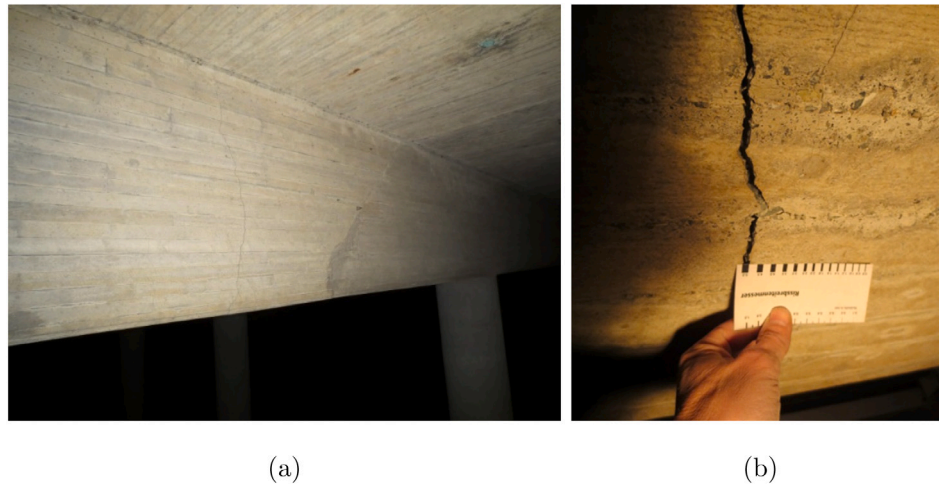


Fig. 13. Vertical crack in a region with low amount of reinforcement in (a), which is measured in (b). Image courtesy of Dr. Ing. A. Aas-Jakobsen AS.

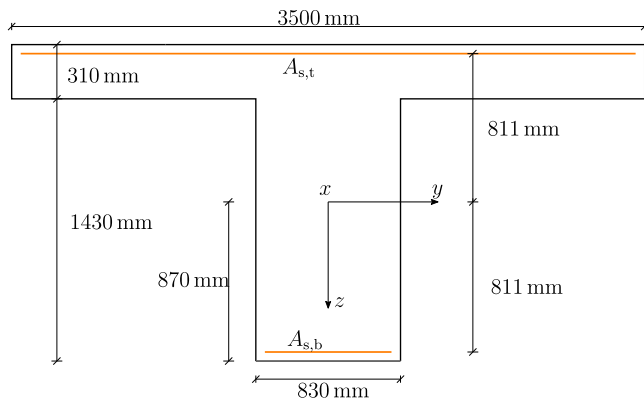


Fig. 14. Geometry of the beam cross section. The  $xy$ -plane is placed in half the height of the beam.

Table 2

Reinforcement layout. The coordinate is the distance from the leftmost support, and  $A_{s,b}$  and  $A_{s,t}$  are the reinforcement areas in the bottom and top of the cross-section (see Fig. 14).

Coordinate [mm]	$A_{s,b}$ [mm <sup>2</sup> ]	$A_{s,t}$ [mm <sup>2</sup> ]
0–4500	2412.7	27344.4
4500–8500	12063.7	4021.2
8500–14000	15280.7	4021.2
14000–18000	12063.7	4021.2
18000–22500	2412.7	27344.4
22500–27000	2412.7	27344.4
27000–31000	12063.7	4021.2
31000–36500	15280.7	4021.2
36500–40500	12063.7	4021.2
40500–45000	12063.7	30561.4
45000–49000	12063.7	30561.4
49000–52000	8846.7	4021.2
52000–53500	12063.7	4021.2
53500–62000	20106.2	4021.2
62000–64000	13672.2	4021.2
64000–66250	9651	4021.2

expansion of the bridge of 0.1% (as reasoned in the previous section). Several free ASR strain fields can lead to the same end displacement, and therefore, constraints on the free ASR strain must be given. The free ASR strain field is constrained to a function that is linear in the vertical coordinate  $z$ , and constant along the length of the beam, given

Table 3

Overview of the final free ASR strain gradient  $\kappa^{\text{asr,free}}$  that is applied in each load combination (LC).

Load combination (LC)	$\kappa^{\text{asr,free}}$
LC U	0
LC G	$\frac{-2}{3h} \epsilon_0^{\text{asr,free}}$

by

$$\epsilon^{\text{asr,free}}(z, t) = \frac{t}{t_{\text{end}}} (\epsilon_0^{\text{asr,free}} + \kappa^{\text{asr,free}} z), \quad (33)$$

where  $\epsilon_0^{\text{asr,free}}$  is the final (when  $t = t_{\text{end}}$ ) free ASR strain at the reference axis, and  $\kappa^{\text{asr,free}}$  is the final vertical ASR strain gradient. The strain field (given in Eq. (33)) is also linear in time  $t$ , which might not be realistic, see e.g. [2]. Nevertheless, for simplicity and lack of data necessary for modelling its evolution in time, the linear relation is selected—a particular non-linear evolution would be an equally random choice. Considering the load effects, is the evolution in time only important when the material is assumed time dependent, i.e. when the creep deformation is modelled with linear ageing viscoelasticity. The problem is not yet well-posed, so an additional constraint on the gradient of the free ASR strain field,  $\kappa^{\text{asr,free}}$ , is given and defines the investigated load combinations (see also Table 3 for an overview):

- **LC U:** Zero expansion gradient  $\kappa^{\text{asr,free}} = 0$ , i.e. a *uniform* free ASR expansion field.
- **LC G:** Twice as much free ASR strain on the top ( $\epsilon_t^{\text{asr,free}} = \frac{4}{3} \epsilon_0^{\text{asr,free}}$ ) as on the bottom ( $\epsilon_b^{\text{asr,free}} = \frac{2}{3} \epsilon_0^{\text{asr,free}}$ ) of the beam, which gives  $\kappa^{\text{asr,free}} = \frac{-2}{3h} \epsilon_0^{\text{asr,free}}$ ;  $h$  is the height of the beam. In this case, the gradient depends on the strain at the reference axis.

Different material models are investigated. They are given by combinations of the attributes listed in Table 4, where the combinations are illustrated in Fig. 16. In Section 4 (Results), we specify the applied material models by combinations of the abbreviations. For example, the model specified as NL-VE-ASRD includes non-linear material behaviour of concrete and steel, creep modelled with linear ageing viscoelasticity, stress *independent* ASR expansion (SDch or SDlin was not specified), and stiffness damage due to ASR.

Input values to the material models are based on the design information given on drawings of the Elgeseter Bridge, and are listed in Table 5. It should be noted that the Eurocode creep coefficient used in the effective modulus method (given in Table 5) is calculated as  $\phi = \phi(t_{\text{end}} + 28 \text{ d}, 28 \text{ d}) \approx 2$ . Other relevant input parameters are given in Table 6.

**Table 4**  
Material models used to calculate the load effects due to ASR are combinations of these attributes.

Abbreviation	Description
L	Linear short-term behaviour of both concrete and steel. The crack strain is $\epsilon^{cr} = 0$ in Eq. (3), and the elastic compliance of the sound material is constant $C^{\sigma, \text{sound}} = \frac{1}{E_0}$ in Eq. (10). The plastic strain of the reinforcement $\epsilon^{pl} = 0$ .
NL	Non-linear short-term behaviour of both concrete and steel: compressive damage (Section 2.2.2), cracking (Section 2.2.3), and yielding of reinforcement (Section 2.3).
–	No creep; $\epsilon^{\text{creep}} = 0$ in Eq. (3).
$\phi$	Creep deformation is included by the effective modulus method; $\epsilon^{\text{creep}}$ is given by Eq. (24).
VE	Creep is modelled with linear ageing viscoelasticity, using a kelvin chain model (Equation (25)) fitted to the Eurocode creep function, see Section 2.2.5.
–	Stress independent ASR expansion; $\epsilon^{\text{asr}} = \epsilon^{\text{asr, free}}$ .
SDch $_{\sigma_u}$	Stress dependent ASR expansion (Section 2.2.1), using Charlwood's logarithmic weight function with the value of $\sigma_u$ given by the subscript.
SDlin $_{\sigma_u}$	Stress dependent ASR expansion (Section 2.2.1), using the linear weight function with the value of $\sigma_u$ given by the subscript.
–	No stiffness damage due to ASR; $C^{\sigma, \text{asr}} = 0$ in Eq. (10).
ASRD	Stiffness damage due to ASR.

**Table 5**  
Values for the material properties used in the structural analyses.

Material property	Symbol	Value
<i>Concrete</i>		
Concrete cylinder compressive strength	$f_c = f_{cm}$	28 N/mm <sup>2</sup>
Modulus of elasticity at an age of 28 days	$E_0$	23313 N/mm <sup>2</sup>
Concrete tensile strength	$f_{ct}$	2.2 N/mm <sup>2</sup>
Peak short term compressive strain	$\epsilon_{c0}$	0.002
Creep coefficient used in the effective modulus method ( $\phi$ )	$\phi$	2
ASR expansion parameter	$\sigma_u$	{6, 15} N/mm <sup>2</sup>
ASR expansion parameter	$\sigma_L$	0.2 N/mm <sup>2</sup>
ASR stiffness reduction parameter	$\beta_E^{\text{asr}}$	0.0033
<i>Steel</i>		
Modulus of elasticity	$E_s$	200000 N/mm <sup>2</sup>
Initial yield stress	$f_{sy}$	340 N/mm <sup>2</sup>
Hardening modulus	$S$	0.0001 · $E_0$ [N/mm <sup>2</sup> ]

Note: Material data are based on design information given on drawings. The concrete and the reinforcement steel are equivalent to class C25 (cube strength) and St 52, respectively, in the previous Norwegian code for design of concrete structures (NS 3473) [47], which still is used for assessment of existing structures.

**Table 6**  
Values for other input variables.

Description	Symbol	Value
Final time	$t_{\text{end}}$	69 · 365 days
Notional size of the member	$h_0$	700 mm
Relative humidity	$RH$	80%
External load	$q$	86.67 N/mm

## 4. Results

The following definitions for axial force  $N$  and bending moment  $M$  are used:

$$N = \int_A \sigma dA \quad (34)$$

$$M = \int_A (\sigma - \sigma_{\text{avg}}) z dA; \quad \sigma_{\text{avg}} = \frac{N}{A}. \quad (35)$$

These integrals are calculated at the two Gauss integration points of each beam, and then linearly extrapolated to the nodes of which values are used for plotting.

The results are grouped based on the assumed ASR expansion behaviour. In Section 4.1, the imposed ASR strain field is assumed stress independent, which is considered as an engineering approach, as it can

be modelled by an equivalent thermal strain applied to the concrete (not the steel). The results are included to show the consequences of such simplified assumption. In Section 4.2, more experimentally sound expansion behaviours are assumed, where the imposed ASR strain field is assumed stress dependent of varying degree.

### 4.1. Stress independent ASR expansion

All the results shown in this subsection are calculated based on the assumption that the ASR expansion is independent of the stress history, i.e. the imposed ASR strain equals the free ASR expansion field  $\epsilon^{\text{asr}} = \epsilon^{\text{asr, free}}$  for the whole domain. Figs. 17–18 show the bending moment after permanent load by the black line, and the additional bending moments due to ASR expansion for LC U (in blue) and LC G (in red) calculated with the material models specified in the legend. The results are grouped in Figs. 17 and 18 for material models with linear (L) and non-linear (NL) short-term behaviour of concrete and steel, respectively. When the imposed ASR expansion is uniform (LC U), there is no influence of stiffness on the calculated bending moment. However, the value of  $\epsilon_0^{\text{asr, free}}$  is different, where  $\epsilon_0^{\text{asr, free}}$  increases with decreasing stiffness, as seen in Table 7. In contrast, when the imposed ASR expansion vary linearly over the height (LC G), there is a significant influence of stiffness on the calculated bending moment, as long as linear behaviour (L) is assumed. As seen in Fig. 18, the

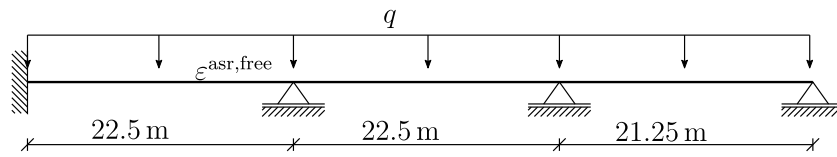


Fig. 15. Beam model of the last three spans of Elgeseter Bridge in Norway.

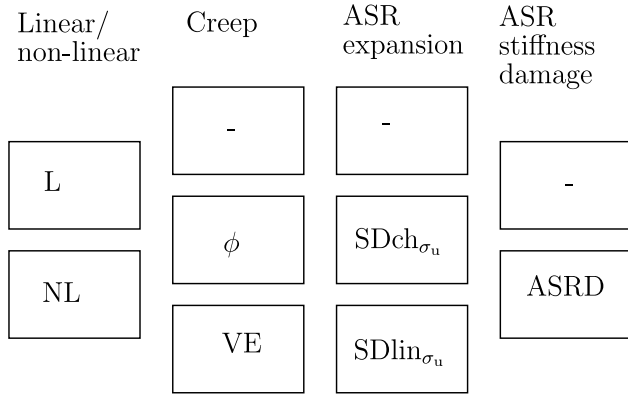


Fig. 16. The investigated material models are combinations of the features (described in Table 4), where one feature (“box”) in each column is combined.

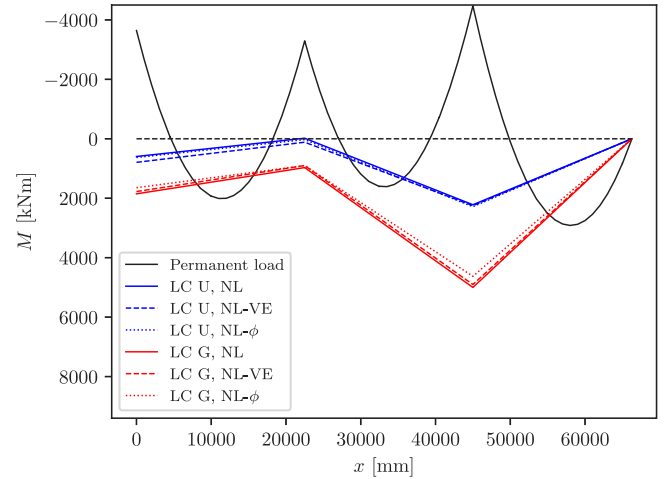


Fig. 18. Bending moment from permanent load, and additional bending moments due to ASR for LC U and LC G when assuming stress independent ASR expansion, and material non-linearity.

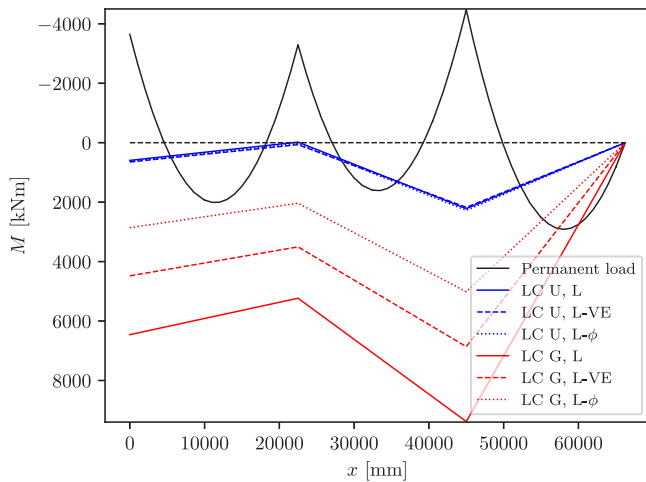


Fig. 17. Bending moment from permanent load, and additional bending moments due to ASR for LC U and LC G when assuming stress independent ASR expansion, and no material non-linearity.

stiffness effect disappear when non-linearities, as concrete cracking and reinforcement yielding, are included.

Cracking and yielding of reinforcement after application of permanent load is plotted in Fig. 19 for the analysis with material model NL. The situation after application of uniform free ASR strain (LC U) is shown in Fig. 20, where one can see that almost all cracks are closed and no reinforcement yielding is present. In contrast, one observes for the case with ASR strain gradient (LC G), in Fig. 21, that substantially more cracking is present, addition to yielding of the reinforcement. The reinforcement yields at three locations (three plastic hinges), where the amount of reinforcement is low. The additional cracks, due to ASR, shown in Fig. 21 are indeed through-cross-section-cracks, and should not be confused with surface cracks due differential ASR expansions through the cross section.

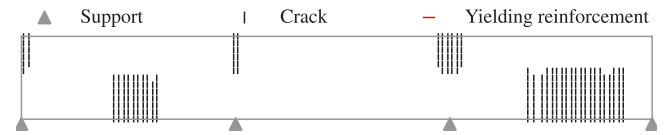


Fig. 19. Open cracks and steel plasticity after application of permanent load. The material model used is NL.

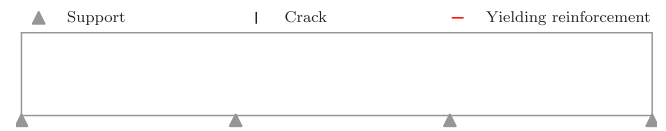


Fig. 20. Open cracks and steel plasticity after ASR expansion, LC U (uniform ASR expansion). The material model used is NL.

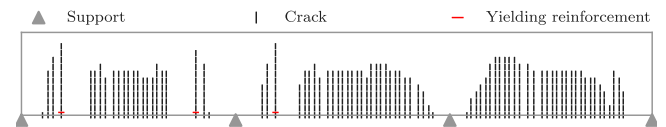


Fig. 21. Open cracks and steel plasticity after ASR expansion, LC G (with ASR strain gradient). The material model used is NL.

#### 4.2. Stress dependent ASR expansion of varying degree

In this subsection, results from analyses with material models where ASR expansion is dependent on the stress are presented (see Section 2.2.1). In these analyses, the imposed ASR strain field is different from the free ASR strain field ( $\epsilon^{asr} \neq \epsilon^{asr,free}$ ). This is clearly shown in Figs. 22 and 23; sub-figure (a) shows the position of two cross sections where the imposed ASR expansion, the concrete stress and the reinforcement stress over the height are plotted in sub-figures (b)–(d). The results in Fig. 22 were obtained with the logarithmic function  $W_{ch}$

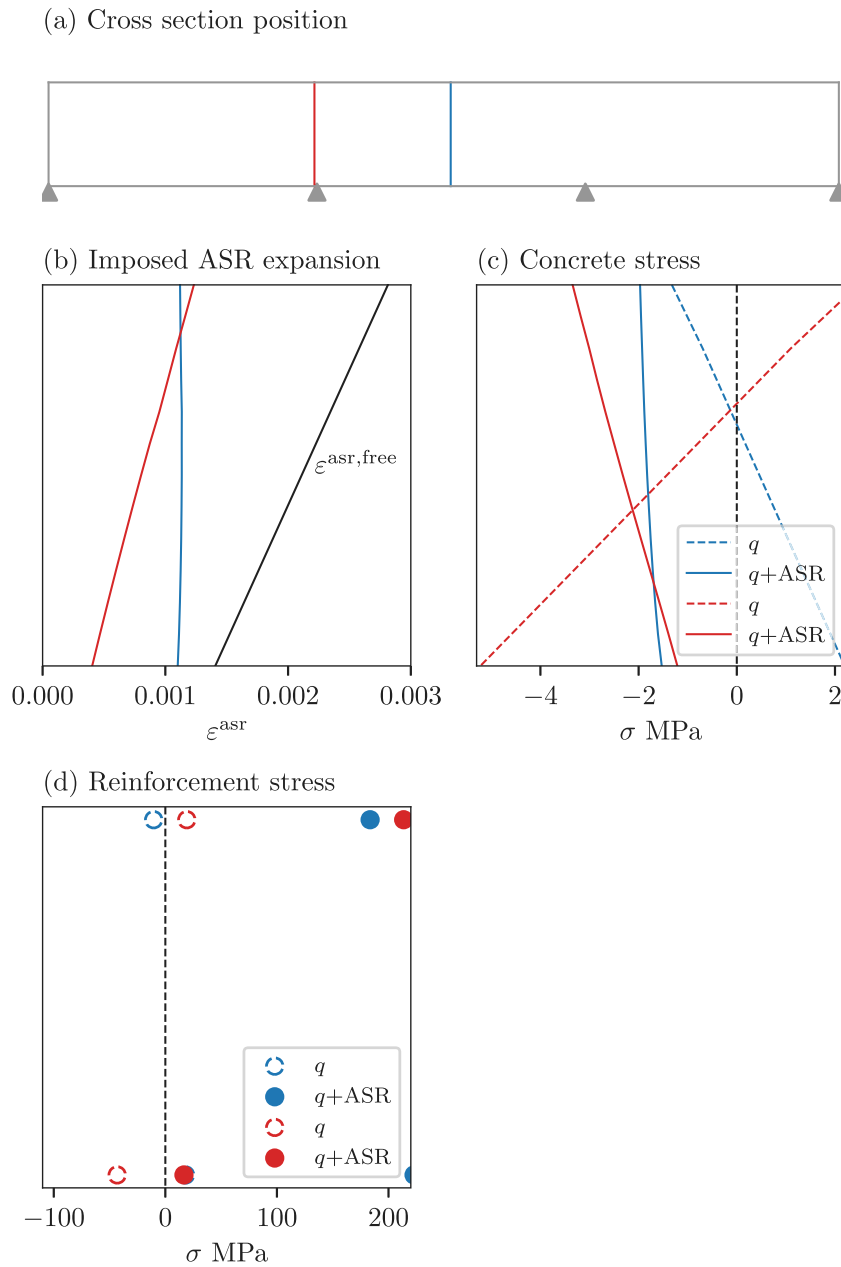


Fig. 22. Cross sectional results from analysis of LC G with material model L-VE-SDch<sub>6</sub> ( $\sigma_u = 6 \text{ N/mm}^2$ ); (a) the locations of the two cross sections; (b) the free and the imposed ASR strain over the height; (c) the concrete stress over the height after permanent load  $q$  (dashed lines) and after ASR expansion (solid lines).

Table 7

The final free ASR strain at the reference axis  $\epsilon_0^{\text{asr,free}}$  in LC U & G, calibrated to result in the same elongation of the bridge of 66 mm.

Material model	LC U	LC G
L	0.00109	0.001
L-VE	0.00115	0.00105
L- $\phi$	0.00126	0.00114
NL	0.00109	0.00091
NL-VE	0.00115	0.00098
NL- $\phi$	0.00126	0.00111

(Eq. (6)), and the linear function  $W_{in}$  (Eq. (7)) was used to obtain the results in Fig. 23. The free ASR expansion—calibrated to give the same elongation of the beam/bridge of 66 mm—is different in the two figures, and therefore, must be explained by the shape of the stress-expansion relationship. The free ASR strains are much larger when

the stress dependence is included, compare Table 8 with Table 7. In Figs. 22 and 23, one should notice that the profile of the imposed ASR strain is no longer linear, and that the average slope/gradient has changed—especially in the middle of the span due to compressive stress in the upper part of the cross section from the permanent load. The maximum compressive stress from permanent load (shown with dashed lines in Fig. 22(c)) is smaller than the compressive stress required to stop the ASR expansion  $\sigma_u = 6 \text{ N/mm}^2$ . A post-tensioning effect is also observed, where concrete stress decreases (c) while the reinforcement stress increases (d).

Similar to Section 4.1 (results from simulations with stress independent ASR expansion), there is no influence of concrete stiffness on the bending moments when a uniform free ASR expansion field is applied, as seen in Fig. 24. Even for LC G with free ASR expansion gradient, there is no influence of concrete stiffness when the material model includes stress dependent ASR expansion in accordance with Charlwood’s stress-expansion relationship with  $\sigma_u = 6 \text{ N/mm}^2$ .

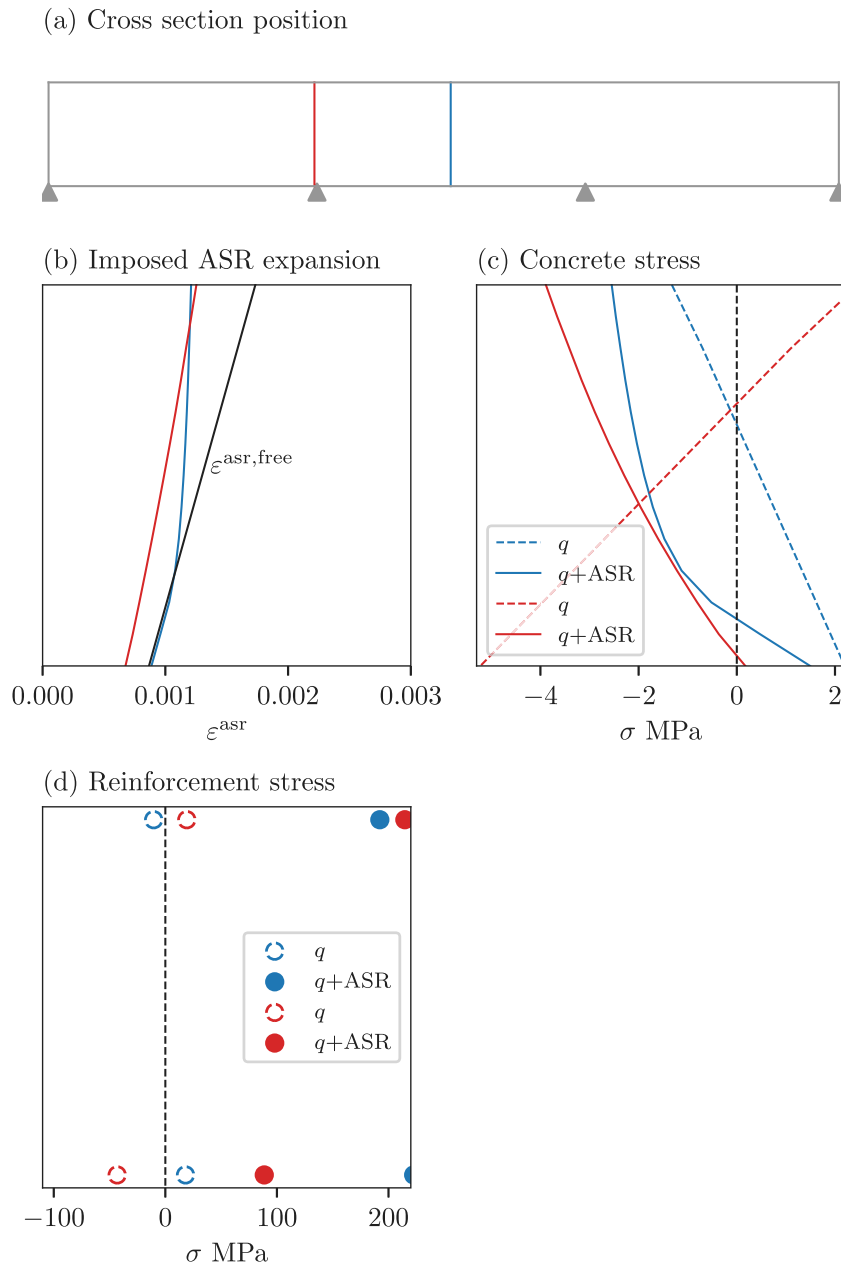


Fig. 23. Cross sectional results from analysis of LC G with material model L-VE-SDlin<sub>6</sub> ( $\sigma_u = 6 \text{ N/mm}^2$ ); (a) the locations of the two cross sections; (b) the free and the imposed ASR strain over the height; (c) the concrete stress over the height after permanent load  $q$  (dashed lines) and after ASR expansion (solid lines).

To study the effect of stress dependent ASR expansion of varying degree, results from both a logarithmic (Charlwood) and a linear stress-expansion relationship  $W$  are presented in Fig. 25 for two values of the material parameter  $\sigma_u = \{6, 15\} \text{ N/mm}^2$ . When the logarithmic stress-expansion relationship is used, there is no evident influence of concrete stiffness, but a slight increase in bending moment when  $\sigma_u$  shifts from  $6 \text{ N/mm}^2$  to  $15 \text{ N/mm}^2$ . Whereas for a linear stress-expansion relationship, the influence of stiffness is clearly observed for both values of  $\sigma_u$ . All the results in Fig. 25 are obtained with linear behaviour of both concrete and steel. The effect of non-linearity (concrete cracking and reinforcement plasticity) for various ASR stress-expansion relationships are shown in Fig. 26. From this figure, it is observed that the difference (in the calculated bending moments) between linear (L) and non-linear (NL) material behaviour increases when the sensitivity of ASR expansion to stress decreases. Similarly, the stress dependency of the ASR expansion also influences the calculated crack pattern, see Fig. 28. Much more cracking is observed for low sensitivity of ASR

Table 8

The final free ASR strain at the reference axis  $\epsilon_0^{\text{asr,free}}$  in LC U & G, calibrated to result in the same elongation of the bridge of 66 mm. The subindices 6 and 15 indicate the value of  $\sigma_u$  to either  $6 \text{ N/mm}^2$  or  $15 \text{ N/mm}^2$ .

Material model	LC U	LC G
L-VE-SDch <sub>6</sub>	0.00225	0.00211
L-VE-SDch <sub>15</sub>	-	0.00173
NL-VE-SDch <sub>6</sub>	0.002254	0.002078
NL-VE-SDch <sub>15</sub>	0.001845	0.0017

expansion to compressive stress (SDlin<sub>15</sub>), than for high sensitivity (SDlin<sub>6</sub>). The effect of ASR stiffness damage is only significant when the ASR expansion has a low sensitivity to stress, i.e. for linear stress-expansion relationship with  $\sigma_u = 15 \text{ MPa}$ , and when linear material behaviour is assumed, see Fig. 27.

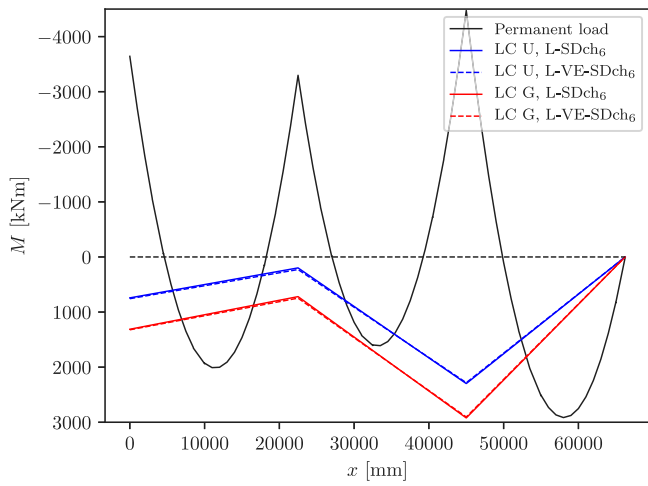


Fig. 24. Bending moment from permanent load (black line) and additional bending moment due to ASR for LC U and G, calculated with stress dependent ASR expansion in accordance with Charwood's stress-expansion relation (SDch) with  $\sigma_u = 6 \text{ N/mm}^2$ . Material models: L-SDch<sub>6</sub> and L-VE-SDch<sub>6</sub>.

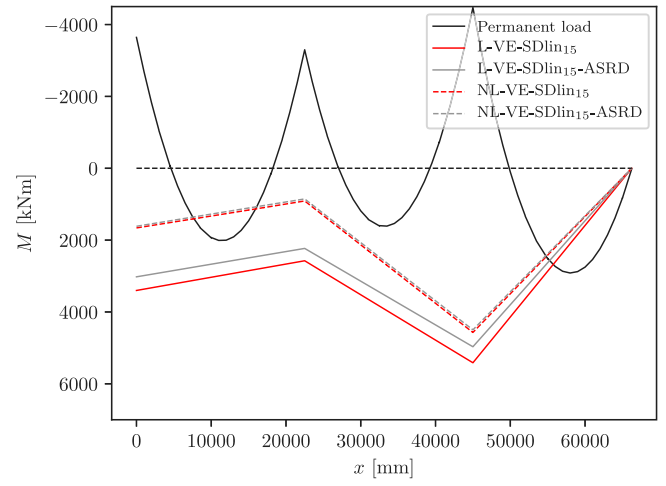


Fig. 27. Bending moment from permanent load (black line) and additional bending moment due to ASR for LC G, calculated with material models with linear stress ASR expansion relationship with  $\sigma_u = 15 \text{ N/mm}^2$ , in combination with linear (L) and non-linear (NL) material behaviour and ASR stiffness damage.

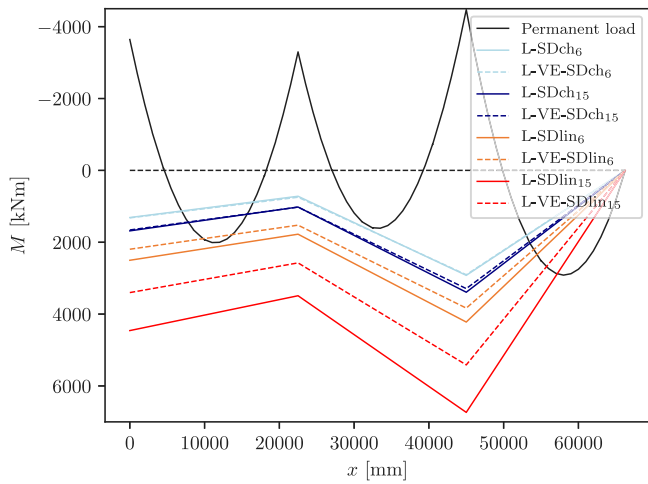


Fig. 25. Bending moment from permanent load (black line) and additional bending moment due to ASR for LC G, calculated with material models with stress dependent ASR expansion of varying degree.

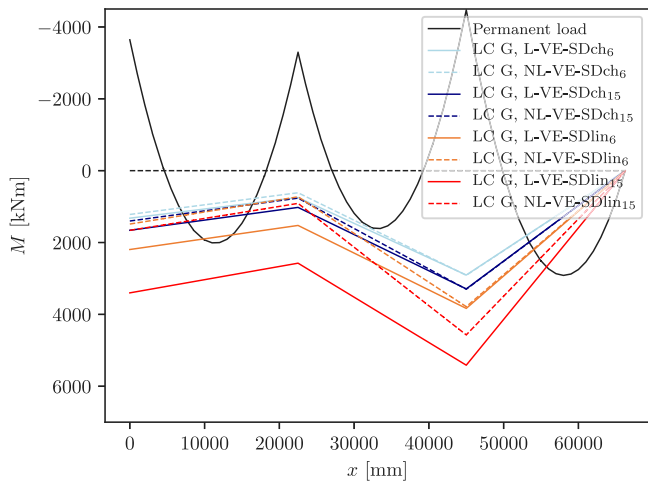


Fig. 26. Bending moment from permanent load (black line) and additional bending moment due to ASR for LC G, calculated with material models with two stress ASR expansion relationships, in combination with linear (solid lines) and non-linear (dashed lines) material behaviour of concrete and steel.

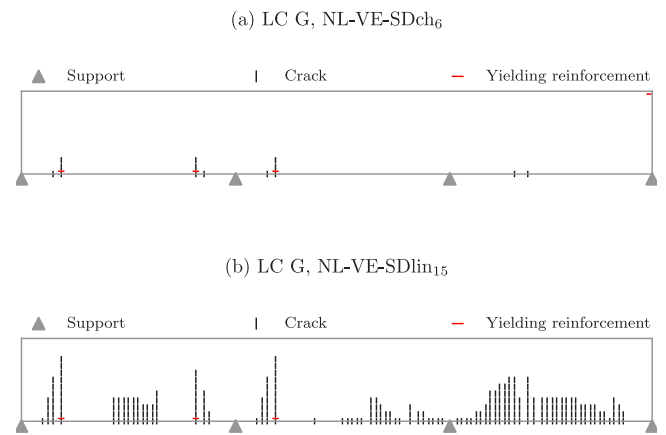


Fig. 28. Open cracks and reinforcement yielding after ASR expansion for LC G, obtained with two different ASR stress-expansion relationships: (a) Charwood's logarithmic function with  $\sigma_u = 6 \text{ MPa}$ , and (b) linear function with  $\sigma_u = 15 \text{ MPa}$ .

### 5. Discussion

Substantial additional stresses occur in an ordinary RC beam subjected to an imposed ASR strain. If the beam structure is statically determinate, self-equilibrating stresses occur, where the reinforcement stress increases while the concrete stress decreases. However, the net cross-sectional forces, axial force and bending moment, do not change. In contrast, if the beam structure is statically indeterminate, additional cross-sectional forces occur if the displacements, caused by the ASR-induced expansion, are restrained at the supports, or restrained by other structural parts. The three-span beam investigated in this study is statically indeterminate, and additional bending moments occur. Because the structural system allows for axial displacement, no axial force arises. Unlike a uniform thermal expansion, gives a uniform imposed ASR expansion additional bending moments. This is due to an expanding concrete that is restrained by an asymmetric reinforcement layout (more/less in the top than in the bottom of the cross sections), which causes curvature (vertical expansion gradient) of each cross section, and as a result, vertical displacements. This kind of ASR-induced curvature is also experimentally observed in thick concrete slabs with asymmetric reinforcement [48]. The reinforcements have two effects on the total expansion field (which explain the imposed

expansion gradients): (1) mechanical (elastic) effect due to (ASR) strain incompatibility between concrete and reinforcement, which reduces the concrete stress and increases the reinforcement stress; and (2) a secondary effect if the concrete is brought to compression, as compression decreases the imposed ASR expansion. In all of our calculations, the first effect of reinforcement is included, and when ASR expansion is assumed dependent on stress, also the second effect is accounted for.

For now, let us assume that the ASR expansion is independent of stress  $\epsilon^{\text{asr}} = \epsilon^{\text{asr,free}}$ . Then, from Figs. 17 and 18, we can note two important observations: (1) an imposed ASR strain gradient (LC G) results in a significant increase in bending moment compared to the uniform case (LC U), and (2) only when an expansion gradient is imposed, there is an influence of concrete stiffness, where the lower the stiffness the lower the bending moment. It should be noted that the result obtained with the linear ageing viscoelastic material model (L-VE), which gives the most accurate description of creep, is in between the results for the linear elastic material model with initial modulus of elasticity (L) and with effective modulus of elasticity (L- $\phi$ ). The two methods to include concrete creep strain give very different results, and can be explained by the slow development of ASR-induced stresses (69 years). The slow development is accounted for when using the ageing viscoelastic material model, but not when using the effective modulus method, as the creep coefficient for the effective modulus method was calculated based on the assumption of loading—including imposed ASR expansion—at concrete age of 28 days. Besides, the ageing effect (illustrated in Fig. 8) is important, as late ASR-induced stress causes less maximum creep strain than early ASR-induced stress.

By comparing Fig. 17 with 18, one observes a great difference in the calculated bending moment for the LC with expansion gradient (LC G). When cracking and steel plasticity (NL) are included in the analyses (Fig. 18), the calculated bending moments drop, and the influence of the stiffness of the concrete vanishes. This is due to extensive cracking (and yielding) of the concrete at three locations where the amount of reinforcement is low, see Fig. 21. As plastic hinges develop, the bending moments are limited by the moment capacity of these weak cross sections, and therefore, the concrete stiffness has minor influence on the final calculated bending moment. However, there are still differences in other variables, e.g. displacement, crack- and plastic strains. Small amount of reinforcement at these locations are typical for bridge structures, as the reinforcement layout is designed based on the bending moment distribution from standard vertical loading (permanent loads, and traffic loads).

When stress dependent ASR expansion is included in the material model, the imposed ASR strain field  $\epsilon^{\text{asr}}$  is different from the free ASR strain field  $\epsilon^{\text{asr,free}}$ , where the deviation depends on the value of the material parameter  $\sigma_u$  and the shape of the function  $W$ . This stress dependency reduces the ASR-induced bending moment for the load case with a gradient in the free ASR strain field (LC G); compare e.g. the bending moment calculated with L-VE in Fig. 17 with the bending moment calculated with L-VE-SDch<sub>6</sub> in Fig. 24. This is explained by the reduction in the average gradient of the imposed ASR strain field, as seen in Figs. 22 and 23. This is most evident in the middle of the spans due to the stress state from permanent load (before ASR expansion takes place). In the middle of the spans, there is compressive stress in the upper part of the cross section from permanent load, which reduce the ASR expansion, and consequently the gradient. It is interesting to note that the results from the load case with free ASR strain gradient (LC G) approach the results from the load case with uniform free ASR strain (LC U) as the sensitivity of ASR expansion to compressive stress increases, see Fig. 29. Furthermore, for the load case with uniform free ASR strain (LC U), there is no clear difference in the calculated bending moment when analysed with material models *with* and *without* stress dependent ASR expansion. This is because almost the same *imposed* ASR strain field ( $\epsilon^{\text{asr}}$ ) is present for both cases, but the *free* ASR strain field ( $\epsilon^{\text{asr,free}}$ ) is different.

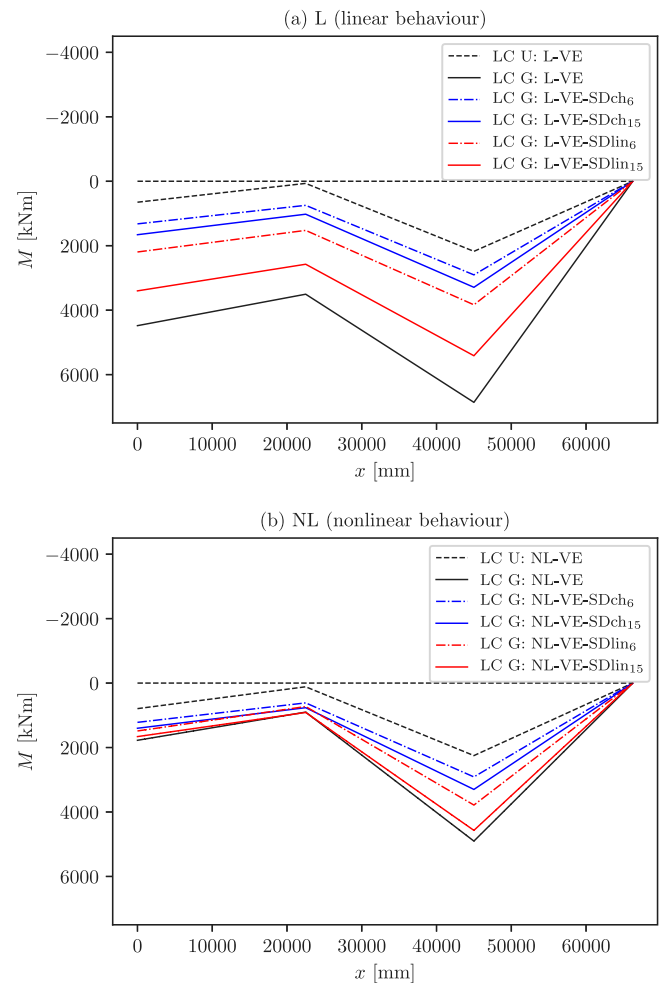


Fig. 29. Additional bending moment due to ASR. Linear short-term behaviour of concrete and steel in (a), while non-linear (including cracking, compressive damage, and reinforcement yielding) behaviour in (b).

The free ASR strain represents the expansion that would occur without stress. Experimental studies show that it depends on the concrete mix, and the exposure conditions as temperature and relative humidity. In our study, it should be noted that the final free ASR expansion  $\epsilon_0^{\text{asr,free}}$  is obtained by inverse analysis from the elongation measurement of the bridge. Consequently, it depends on the choice of material model, and in particular, on the choice of expansion model, compare the results in Tables 8 and 7. If the free expansion behaviour of the concrete in question is available, one can assess whether the free expansions that are obtained through inverse structural analyses are reasonable.

In this study, bending moment was used as a measure for the ASR-induced stresses. It is emphasized that it is an integrated quantity of both concrete and reinforcement stress over the cross section, and thus does not provide any information on the stress distribution within the cross section. Information on the stress distribution may be of importance when assessing the structural capacity. The expanding concrete and the non-expanding reinforcement result in a substantial increase in reinforcement strain and stress, as seen in Fig. 22, which may influence the bending resistance of the cross section against further loading. Further study of the consequence of ASR on the structural capacity of continuous beams/bridges is recommended. Furthermore, it should be studied whether the two-step procedure used in design is applicable for structural reassessment of ASR-affected RC structures.

## 6. Conclusion

The structural effects of ASR expansion in ordinary RC beam bridges were studied, using Euler–Bernoulli beam theory. Based on a real case, Elgeseter Bridge in Norway, a simplified case was constructed: a three-span beam that is affected by ASR to varying extent. From a numerical study, using non-linear finite element analyses, of the beam, the following conclusions are drawn:

- Uniform imposed ASR expansion causes additional bending moments. This is explained by an asymmetric reinforcement layout with respect to the neutral axis, which causes cross sectional rotations and vertical displacement of the beam when concrete expands. As the displacements are restrained at the supports, reaction forces and bending moments occur.
- Significantly greater load effects occur with an imposed ASR strain gradient.
- In the case of a gradient in the free ASR expansion, with larger expansion in slab than in the web, the stress dependency of ASR expansion has a reducing effect on the calculated bending moments. This is explained by a reduction in the average gradient of the imposed ASR strain field. However, it should be noted that this conclusion is drawn based on the assumed expansion behaviour, i.e. the expansion in the longitudinal direction of the beam depends only on the free ASR expansion and the stress in the same direction. Other anisotropic expansion behaviours may lead to different results, which can only be answered with 3D analysis.
- Cracking of concrete and yielding of reinforcement, results in development of plastic (crack) hinges, which release the stresses in the system, thus lowering the calculated bending moments.
- For the investigated structural system, creep and ASR damage (the concrete stiffness) are only important, with respect to the calculated bending moments, when there exists an imposed ASR strain gradient, and when plastic (crack) hinges do not develop.

The most advanced model, and upon an adequate estimation of the material parameters and the free ASR strain gradient, is a model that includes cracking, compressive damage, creep, stress dependent ASR expansion, and ASR stiffness damage. From the consulting engineer perspective is the linear structural analysis—based on linear material behaviour—the preferred approach for both design and assessment of existing structures. It is emphasized that the linear approach may give too high load effects when an imposed ASR strain gradient is assumed. In order to avoid unnecessary disapproval of continuous beam bridges suffering from ASR, the linear analysis should be conducted with great care. The measures to solve the problem include reduction of stiffness due to cracking and reinforcement yielding, and reduction of the imposed ASR gradient.

## CRedit authorship contribution statement

**Simen Sørsgaard Kongshaug:** Conceptualization, Methodology, Software, Formal analysis, Writing – original draft, Investigation, Writing – review & editing, Visualization. **Rolf Magne Larssen:** Conceptualization, Methodology, Writing – review & editing. **Max A.N. Hendriks:** Writing – review & editing, Supervision. **Terje Kanstad:** Writing – review & editing, Supervision. **Gro Markeset:** Conceptualization, Methodology, Writing – review & editing, Supervision.

## Declaration of competing interest

The authors declare that they have no known competing financial interests or personal relationships that could have appeared to influence the work reported in this paper.

## References

- [1] Swamy R, Al-Asali M. Engineering properties of concrete affected by alkali-silica reaction. *Mater J* 1988;85(5):367–74.
- [2] Larive C. Apports combinés de l'expérimentation et de la modélisation à la compréhension de l'alkali-réaction et de ses effets mécaniques [Ph.D. thesis], Ecole nationale des ponts et chaussées; 1997.
- [3] Giaccio G, Zerbino R, Ponce J, Batic OR. Mechanical behavior of concretes damaged by alkali-silica reaction. *Cem Concr Res* 2008;38(7):993–1004.
- [4] Esposito R, Anaç C, Hendriks MA, Çopuroğlu O. Influence of the alkali-silica reaction on the mechanical degradation of concrete. *J Mater Civ Eng* 2016;28(6):04016007.
- [5] Jensen V. Alkali-silica reaction damage to Elgeseter Bridge, Trondheim, Norway: a review of construction, research and repair up to 2003. *Mater Charact* 2004;53(2):155–70. <http://dx.doi.org/10.1016/j.matchar.2004.09.006>, eMABM 2003: 9th Euroseminar on Microscopy Applied to Building Materials. URL <https://www.sciencedirect.com/science/article/pii/S1044580304002086>.
- [6] Courtier R. The assessment of ASR-affected structures. *Cem Concr Compos* 1990;12(3):191–201. [http://dx.doi.org/10.1016/0958-9465\(90\)90020-X](http://dx.doi.org/10.1016/0958-9465(90)90020-X), URL <https://www.sciencedirect.com/science/article/pii/095894659090020X>.
- [7] Charlowood R, Solymar S, Curtis D. A review of alkali aggregate reactions in hydroelectric plants and dams. In: Proceedings of the international conference of alkali-aggregate reactions in hydroelectric plants and dams, vol. 129. 1992.
- [8] Wen HX. Prediction of structural effects in concrete affected by alkali-aggregate reaction [Ph.D. thesis], University of Plymouth; 1993.
- [9] Léger P, Côté P, Tinawi R. Finite element analysis of concrete swelling due to alkali-aggregate reactions in dams. *Comput Struct* 1996;60(4):601–11. [http://dx.doi.org/10.1016/0045-7949\(95\)00440-8](http://dx.doi.org/10.1016/0045-7949(95)00440-8), URL <https://www.sciencedirect.com/science/article/pii/0045794995004408>.
- [10] Multon S, Seignol J-F, Toutlemonde F. Chemo-mechanical assessment of beams damaged by alkali-silica reaction. *J Mater Civ Eng* 2006;18(4):500–9. [http://dx.doi.org/10.1061/\(ASCE\)0899-1561\(2006\)18:4\(500\)](http://dx.doi.org/10.1061/(ASCE)0899-1561(2006)18:4(500)).
- [11] Saouma V, Perotti L. Constitutive model for alkali-aggregate reactions. *Mater J* 2006;103(3):194–202.
- [12] Pan J, Feng Y, Wang J, Sun Q, Zhang C, Owen D. Modeling of alkali-silica reaction in concrete: a review. *Front Struct Civ Eng* 2012;6(1):1–18.
- [13] Esposito R, Hendriks M. Literature review of modelling approaches for ASR in concrete: a new perspective. *Eur J Environ Civ Eng* 2017;1–21.
- [14] Eurocode 2: Design of concrete structures. Part 1-1: General rules and rules for buildings (EN 1992-1-1:2004). 2004.
- [15] Jones A, Clark L. The effects of restraint on ASR expansion of reinforced concrete. *Mag Concr Res* 1996;48(174):1–13.
- [16] Multon S, Toutlemonde F. Effect of applied stresses on alkali-silica reaction-induced expansions. *Cem Concr Res* 2006;36(5):912–20.
- [17] Berra M, Faggiani G, Mangialardi T, Paolini A. Influence of stress restraint on the expansive behaviour of concrete affected by alkali-silica reaction. *Cem Concr Res* 2010;40(9):1403–9. <http://dx.doi.org/10.1016/j.cemconres.2010.05.002>, URL <https://www.sciencedirect.com/science/article/pii/S0008884610001213>.
- [18] Kagimoto H, Yasuda Y, Kawamura M. ASR expansion, expansive pressure and cracking in concrete prisms under various degrees of restraint. *Cem Concr Res* 2014;59:1–15.
- [19] Liaudat J, Carol I, López CM, Saouma VE. ASR expansions in concrete under triaxial confinement. *Cem Concr Compos* 2018;86:160–70.
- [20] Kongshaug SS, Oseland O, Kanstad T, Hendriks MA, Rodum E, Markeset G. Experimental investigation of ASR-affected concrete—The influence of uniaxial loading on the evolution of mechanical properties, expansion and damage indices. *Constr Build Mater* 2020;245:118384.
- [21] Herrador MF, Martínez-Abella F, Dopico JRR. Experimental evaluation of expansive behavior of an old-aged ASR-affected dam concrete: methodology and application. *Mater Struct* 2008;41(1):173–88.
- [22] Multon S, Seignol JF, Toutlemonde F. Structural behavior of concrete beams affected by alkali-silica reaction. *ACI Mater J* 2005;102(2):67, Name - American Concrete Pavement Association; Copyright - Copyright American Concrete Institute Mar/Apr 2005; Document feature - Diagrams; Tables; Equations; Graphs; ; Last updated - 2010-06-06. URL <https://search.proquest.com/scholarly-journals/structural-behavior-concrete-beams-affected/docview/198091717/se-2?accountid=12870>.
- [23] Ulm F-J, Coussy O, Kefei L, Larive C. Thermo-chemo-mechanics of ASR expansion in concrete structures. *J Eng Mech* 2000;126(3):233–42.
- [24] Comi C, Kirchmayr B, Pignatelli R. Two-phase damage modeling of concrete affected by alkali-silica reaction under variable temperature and humidity conditions. *Int J Solids Struct* 2012;49(23):3367–80.
- [25] Comi C, Fedele R, Perego U. A chemo-thermo-damage model for the analysis of concrete dams affected by alkali-silica reaction. *Mech Mater* 2009;41(3):210–30.
- [26] Pourbehi MS, van Zijl GPAG. Seismic analysis of the kleinplaas dam affected by alkali-silica reaction using a chemo-thermo-mechanical finite element numerical model considering fluid structure interaction. *J Adv Concr Technol* 2019;17(8):462–73. <http://dx.doi.org/10.3151/jact.17.462>.

- [27] Capra B, Sellier A. Orthotropic modelling of alkali-aggregate reaction in concrete structures: numerical simulations. *Mech Mater* 2003.
- [28] Morenon P, Multon S, Sellier A, Grimal E, Hamon F, Kolmayer P. Flexural performance of reinforced concrete beams damaged by Alkali-Silica Reaction. *Cem Concr Compos* 2019;104:103412. <http://dx.doi.org/10.1016/j.cemconcomp.2019.103412>, URL <https://www.sciencedirect.com/science/article/pii/S0958946519303348>.
- [29] Gorga R, Sanchez L, Martín-Pérez B. FE approach to perform the condition assessment of a concrete overpass damaged by ASR after 50 years in service. *Eng Struct* 2018;177:133–46.
- [30] Østmoen T. Elgeseter bridge – Report from special survey in 2012. Tech. rep., Dr. Ing. A. Aas-Jakobsen AS; 2013 [in Norwegian].
- [31] Rodum E, Pedersen BM, Relling RH. Field and laboratory examinations of an ASR-affected bridge—variation in crack extent and water content. In: 15th ICAAR Conference. 2016.
- [32] Larssen RM. Elgeseter bridge – Statical classification and strengthening. Tech. rep., Dr. Ing. A. Aas-Jakobsen AS; 2014 [in Norwegian].
- [33] Stemland H, Rodum E, Johansen H. ASR – Guidance for structural analysis. Tech. rep. 601, Norwegian Public Roads Administration; 2016 [in Norwegian].
- [34] Van Zijl G, De Borst R, Rots J. A numerical model for the time-dependent cracking of cementitious materials. *Internat J Numer Methods Engrg* 2001;52(7):637–54.
- [35] Van Zijl G, De Borst R, Rots J. The role of crack rate dependence in the long-term behaviour of cementitious materials. *Int J Solids Struct* 2001;38(30–31):5063–79.
- [36] Gautam B, Panesar D, Sheikh S, Vecchio F. Effect of multiaxial stresses on alkali-silica reaction damage of concrete. *Materials* 2017;114:595–604.
- [37] Hayes NW, Gui Q, Abd-Elssamad A, Le Pape Y, Giorla AB, Le Pape S, Giannini ER, Ma ZJ. Monitoring alkali-silica reaction significance in nuclear concrete structural members. *J Adv Concr Technol* 2018;16(4):179–90.
- [38] Gravel C, Ballivy G, Khayat K, Quirion M, Lachemi M. Expansion of AAR concrete under triaxial stresses: Simulation with instrumented concrete block. In: Proc. 11th int. conf. AAR. 2000, p. 949–58.
- [39] Ahmed TMA, Burley E, Rigden SR. The effect of alkali—silica reaction on the fatigue behaviour of plain concrete tested in compression, indirect tension and flexure. *Mag Concr Res* 1999;51(6):375–90. <http://dx.doi.org/10.1680/mac.1999.51.6.375>, URL [arXiv:https://doi.org/10.1680/mac.1999.51.6.375](https://doi.org/10.1680/mac.1999.51.6.375).
- [40] Dunant CF, Scrivener KL. Effects of uniaxial stress on alkali-silica reaction induced expansion of concrete. *Cem Concr Res* 2012;42(3):567–76. <http://dx.doi.org/10.1016/j.cemconres.2011.12.004>, URL <https://www.sciencedirect.com/science/article/pii/S0008884611003267>.
- [41] Sanchez L, Fournier B, Jolin M, Bastien J. Evaluation of the stiffness damage test (SDT) as a tool for assessing damage in concrete due to ASR: Test loading and output responses for concretes incorporating fine or coarse reactive aggregates. *Cem Concr Res* 2014;56:213–29. <http://dx.doi.org/10.1016/j.cemconres.2013.11.003>, URL <http://www.sciencedirect.com/science/article/pii/S0008884613002287>.
- [42] Grimal E, Sellier A, Le Pape Y, Bourdarot E. Creep, shrinkage, and anisotropic damage in alkali-aggregate reaction swelling mechanism-part I: A constitutive model. *Mater J* 2008;105(3):227–35.
- [43] Morenon P, Multon S, Sellier A, Grimal E, Hamon F, Bourdarot E. Impact of stresses and restraints on ASR expansion. *Constr Build Mater* 2017;140:58–74.
- [44] Pourbehi MS, van Zijl GP, et al. Analysis of combined action of seismic loads and alkali-silica reaction in concrete dams considering the key chemical-physical-mechanical factors and fluid-structure interaction. *Eng Struct* 2019;195:263–73.
- [45] Popovics S. A numerical approach to the complete stress-strain curve of concrete. *Cem Concr Res* 1973;3(5):583–99. [http://dx.doi.org/10.1016/0008-8846\(73\)90096-3](http://dx.doi.org/10.1016/0008-8846(73)90096-3), URL <http://www.sciencedirect.com/science/article/pii/0008884673900963>.
- [46] Reinhardt HW, Özkan H, Mielich O. Changes in mechanical properties of concrete due to ASR. *Hormigón Y Acero* 2018;69:15–9. <http://dx.doi.org/10.1016/j.hya.2018.02.001>, URL <https://www.sciencedirect.com/science/article/pii/S0439568918300172>.
- [47] NS 3473:2003 concrete structures - Design and detailing rules. 2003 [in Norwegian].
- [48] Allard A, Bilodeau S, Pissot F, Fournier B, Bastien J, Bissonnette B. Expansive behavior of thick concrete slabs affected by alkali-silica reaction (ASR). *Constr Build Mater* 2018;171:421–36. <http://dx.doi.org/10.1016/j.conbuildmat.2018.03.159>, URL <https://www.sciencedirect.com/science/article/pii/S0950061818306585>.